The Community Climate System Model Version 3 (CCSM3)

WILLIAM D. COLLINS,* CECILIA M. BITZ,+ MAURICE L. BLACKMON,* GORDON B. BONAN,* CHRISTOPHER S. BRETHERTON,+ JAMES A. CARTON,# PING CHANG,@ SCOTT C. DONEY,& JAMES J. HACK,* THOMAS B. HENDERSON,* JEFFREY T. KIEHL,* WILLIAM G. LARGE,* DANIEL S. MCKENNA,* BENJAMIN D. SANTER,** AND RICHARD D. SMITH++

*National Center for Atmospheric Research, Boulder, Colorado
+ University of Washington, Seattle, Washington
# University of Maryland, College Park, College Park, Maryland
@ Texas A&M University, College Station, Texas
& Woods Hole Oceanographic Institution, Woods Hole, Massachusetts
** Lawrence Livermore National Laboratory, Livermore, California
++ Los Alamos National Laboratory, Los Alamos, New Mexico

(Manuscript received 10 February 2005, in final form 1 September 2005)

ABSTRACT

The Community Climate System Model version 3 (CCSM3) has recently been developed and released to the climate community. CCSM3 is a coupled climate model with components representing the atmosphere, ocean, sea ice, and land surface connected by a flux coupler. CCSM3 is designed to produce realistic simulations over a wide range of spatial resolutions, enabling inexpensive simulations lasting several millennia or detailed studies of continental-scale dynamics, variability, and climate change. This paper will show results from the configuration used for climate-change simulations with a T85 grid for the atmosphere and land and a grid with approximately 1° resolution for the ocean and sea ice. The new system incorporates several significant improvements in the physical parameterizations. The enhancements in the model physics are designed to reduce or eliminate several systematic biases in the mean climate produced by previous editions of CCSM. These include new treatments of cloud processes, aerosol radiative forcing, land–atmosphere fluxes, ocean mixed layer processes, and sea ice dynamics. There are significant improvements in the sea ice thickness, polar radiation budgets, tropical sea surface temperatures, and cloud radiative effects. CCSM3 can produce stable climate simulations of millennial duration without ad hoc adjustments to the fluxes exchanged among the component models. Nonetheless, there are still systematic biases in the ocean–atmosphere fluxes in coastal regions west of continents, the spectrum of ENSO variability, the spatial distribution of precipitation in the tropical oceans, and continental precipitation and surface air temperatures. Work is under way to extend CCSM to a more accurate and comprehensive model of the earth's climate system.

1. Introduction

The Community Climate System Model (CCSM) is a coupled model for simulating past, present, and future climates. In its present form, CCSM consists of four components for the atmosphere, ocean, sea ice, and land surface linked through a coupler that exchanges fluxes and state information among these components. It is developed and used by an international community of students and scientists from universities, national laboratories, and other institutions. Applications include studies of interannual and interdecadal variability, simulations of paleoclimate regimes, and projections of future anthropogenic climate change. The most recent version, CCSM3, was released to the climate community on 23 June 2004. The code, documentation, input datasets, and model simulations are freely available from the CCSM Web site (online at http://www.ccsm.ucar.edu/models). This paper describes some of the most important advances in model physics and dynamics, improvements in the simulated climate, and remaining scientific challenges for future development of CCSM.

CCSM3 is the third generation in an ongoing series of

Corresponding author address: Dr. William D. Collins, NCAR, P.O. Box 3000, Boulder, CO 80307.
E-mail: wcollins@ucar.edu

coupled models developed through international collaboration. The first generation, the Climate System Model version 1 (CSM1), was released in 1996 (Boville and Gent 1998). This model was noteworthy since it did not require adjustments to the fluxes exchanged among the physical components in order to simulate stable, relatively drift-free climates. The second generation, the Community Climate System Model version 2 (CCSM2), was released in 2002 (Kiehl and Gent 2004). The climate simulated with CCSM2 exhibits several improvements over the climate generated from CSM1. CCSM2 produces better simulations of extratropical sea surface temperatures, better tropical variability, and more realistic land surface temperatures. However, several important deficiencies prompted a new cycle of development that has resulted in CCSM3. The main model biases in CCSM2 include a double ITCZ and extended cold tongue, overestimation of winter land surface temperatures, underestimation of tropical tropopause temperatures, erroneous cloud response to SST changes, errors in the east Pacific surface energy budget, and underestimation of tropical variability. As we will show, the new model has reduced or eliminated some of these biases. Since CSM1 and CCSM2 are compared in detail by Kiehl and Gent (2004), the discussion here will address the differences in the model formulations and climate simulations between CCSM2 and CCSM3.

This overview and many other papers in this issue will focus on a configuration of CCSM3 with atmosphere and land models on Eulerian spectral grids with T85 wavenumber truncation and ocean and sea ice models on grids with a nominal equatorial resolution of 1° (the appendix). This configuration has been applied to simulations for international climate-change assessments. Lower-resolution versions of CCSM have been created for applications including rapid scientific development, simulations of biogeochemical processes requiring multicentury simulations for equilibration, and studies of deep-time paleoclimate regimes. The sensitivity of the simulated climate to model resolution is examined in detail by Hack et al. (2006), Yeager et al. (2006), Otto-Bliesner et al. (2006), and DeWeaver and Bitz (2006).

Basic features of the mean climate and its stability are discussed in this paper. Comprehensive analyses of the variability and transient behavior of the system are presented in Deser et al. (2006), Alexander et al. (2006), Meehl et al. (2006), and Gent et al. (2006). Major improvements in the component models are outlined in section 2. More complete descriptions of the enhancements in individual components are given elsewhere in this special issue (e.g., Collins et al. 2006a; Danabasoglu et al. 2006). Improvements in the climate simulation and reductions in systematic errors relative to CCSM2 are discussed in section 3. The stability of the mean climate and analysis of secular trends in climate parameters are presented in section 4. Some of the most significant challenges for improving the simulations in future versions of CCSM are discussed in section 5. Plans for further evaluation and development are summarized in section 6.

2. Overview of CCSM3

The CCSM3 system includes new versions of all the component models: the Community Atmosphere Model version 3 (CAM3; Collins et al. 2004, 2006a), the Community Land Surface Model version 3 (CLM3; Oleson et al. 2004; Dickinson et al. 2006), the Community Sea Ice Model version 5 (CSIM5; Briegleb et al. 2004), and the ocean is based upon the Parallel Ocean Program version 1.4.3 (POP; Smith and Gent 2002). New features in each of these components are described below. Each component is designed to conserve energy, mass, total water, and freshwater in concert with the other components.

a. Design for multiple resolutions and formulations of atmospheric dynamics

CCSM3 has been designed to produce simulations with reasonable fidelity over a wide range of resolutions and with a variety of atmospheric dynamical frameworks. This is accomplished by introducing dependence on resolution and dynamics in the time step and 12 other adjustable parameters in CAM3 (Collins et al. 2004). Those parameters affect the physics governing clouds and precipitation and the biharmonic diffusion coefficients for temperature, vorticity, and divergence. The parameter values have been adjusted to yield climate simulations with nearly balanced top-of-model energy budgets and realistic zonal-mean top-of-atmosphere cloud radiative forcing.

The standard version of CAM3 is based upon the Eulerian spectral dynamical core with triangular spectral truncation at 31, 42, and 85 wavenumbers. The zonal resolution at the equator ranges from 3.75° to 1.41° for the T31 and T85 configurations. It is also possible to integrate CCSM3 with a finite-volume dynamical core (Lin and Rood 1996; Lin 2004) at 2° by 2.5° resolution, although at present this variant of CCSM3 is an experimental version requiring further refinement. The vertical dimension is treated using 26 levels with a hybrid terrain-following coordinate. The vertical grid transitions from a pure sigma region in the lowest layer

through a hybrid sigma–pressure region to a pure pressure region above approximately 83 mb. The land model is integrated on the same horizontal grid as the atmosphere, although each grid box is further divided into a hierarchy of land units, soil columns, and plant types. There are 10 subsurface soil layers in CLM3. Land units represent the largest spatial patterns of subgrid heterogeneity and include glaciers, lakes, wetlands, urban areas, and vegetated regions.

The ocean model uses a dipole grid with a nominal horizontal resolution of 3° or 1°. The semianalytic grids have the first pole located at the true South Pole and the second pole located over Greenland (Smith et al. 1995). The vertical dimension is treated using a depth (z) coordinate with 25 levels extending to 4.75 km in the 3° version and 40 levels extending to 5.37 km in the 1° version. The 1° grid has 320 zonal points and 384 meridional points. The spacing of the grid points is 1.125° in the zonal direction and roughly 0.5° in the meridional direction with higher resolution near the equator. The sea ice model is integrated on the same horizontal grid as the ocean model.

The three standard configurations of CCSM combine the T31 CAM/CLM with the 3° POP/CSIM, the T42 CAM/CLM with the 1° POP/CSIM, and the T85 CAM/CLM with the 1° POP/CSIM. For brevity, we will refer to these configurations as low (T31 × 3), intermediate (T42 × 1), and high (T85 × 1) resolution, respectively. This focus of this paper is on the high-resolution configuration. To facilitate its application, the model has been ported to vector supercomputers, scalar supercomputers, and Linux clusters. On an IBM SP4 system, the low-, intermediate-, and high-resolution configurations require 62, 292, and 1146 CPU hours to simulate one year. Further information on the computational performance is given in Yeager et al. (2006).

b. Development of the atmosphere component

The new atmospheric model includes significant changes to the dynamics, cloud and precipitation processes, radiation processes, and treatments of aerosols. The finite-volume dynamical core is now included as a standard option for integrating CAM (Boville and Rasch 2005, personal communication). The tendency equations can be integrated with either process-split or time-split formulations of the numerical difference approximations (Williamson 2002). In the process-split formulation, the dynamics and physics tendencies are both calculated from the same past model state, while in the time-split formulation, the dynamics and physics tendencies are calculated sequentially. The process-split and time-split representation are used for the Eulerian and finite-volume dynamics, respectively. The physics of cloud and precipitation processes has been modified extensively (Boville et al. 2006). The modifications include separate prognostic treatments of liquid and ice condensate; advection, detrainment, and sedimentation of cloud condensate; and separate treatments of frozen and liquid precipitation. The radiation code has been updated with a generalized treatment of cloud geometrical overlap (Collins et al. 2001) and new parameterizations for the longwave and shortwave interactions with water vapor (Collins et al. 2002a, 2006b). The prognostic sulfur cycle developed by Barth et al. (2000) and Rasch et al. (2000) for predicting sulfate aerosols is now a standard option for the model. A prescribed distribution of sulfate, soil dust, carbonaceous species, and sea salt derived from a three-dimensional assimilation (Collins 2001; Rasch et al. 2001) is used to calculate the direct effects of tropospheric aerosols on the radiative fluxes and heating rates (Collins et al. 2002b). The corresponding effects of stratospheric volcanic aerosols are parameterized following Ammann et al. (2003). Indirect effects of aerosols on cloud albedo and cloud lifetime are not incorporated in CAM3.

c. Development of the ocean component

The CCSM3 ocean model has improved physics and numerics, and the implementation and impact of the more important of these improvements are discussed by Danabasoglu et al. (2006). The better numerics include a more efficient solver for the barotropic continuity equation that improves the scalability of the model to large numbers of processors. Also, a shallow bias in the boundary layer depth is substantially reduced using a higher order (quadratic) interpolation scheme in the K-profile parameterization (KPP) of vertical mixing. Improvements in the physical basis of KPP and the introduction of greater consistency in the discretization have both produced a modest deepening of the boundary layer. Instead of the uniform transmission used in CCSM2, the absorption of solar radiation in the upper ocean varies monthly and spatially based on in situ chlorophyll and satellite ocean color observations (Ohlmann 2003). The more ecologically productive midlatitude, coastal, and equatorial oceans absorb more insolation near the surface, while subtropical oceans are more transmissive. In another departure from previous generations of CCSM, a parameterization of double diffusive mixing in the ocean is now included by default in CCSM3 although its effects are quite small (Danabasoglu et al. 2006). The air–sea turbulent fluxes of momentum, heat, and moisture are now computed using the wind vector relative to the

ocean surface current. However, the effects of wind gusts are not included in the turbulent fluxes. The parameterizations of wind gusts are still quite uncertain, and experiments with some of the existing treatments suggest the effects are relatively minor.

d. Development of the land component

The new land model is based upon a nested subgrid hierarchy of scales representing land units, soil or snow columns, and plant functional types (Bonan et al. 2001; Oleson et al. 2004). CCSM3 includes the effects of competition for water among plant functional types in its standard configuration. One of the primary objectives of the land developers has been to reduce the positive continental temperature biases during boreal winter. Modifications to the relationship between snow height and fractional snow coverage, which have a significant impact on land surface albedos (Oleson et al. 2003), have been considered but have not been adopted in CCSM3. The formulation of the biogeophysics has been modified to increase the sensible and latent heat fluxes over sparsely vegetated surfaces. In previous versions of CCSM, the turbulent transfer coefficient between soil and the overlying canopy air has been set to a constant value for dense canopies. The new formulation makes this coefficient dependent on canopy density characterized by leaf and stem area indices (Oleson et al. 2004). The transfer coefficient is used to obtain aerodynamic resistances for heat and moisture that are inputs to the calculations for latent and sensible heat fluxes. Over large areas of Eurasia, these changes result in a reduction in the 2-m air temperature by 1.5–2 K.

e. Development of the sea ice component

The new CSIM includes modifications to the formulation of ice dynamics, sea ice albedos, and exchanges of salt between sea ice and the surrounding ocean. The horizontal advection of sea ice is now treated with incremental remapping, a more accurate and efficient scheme than that used in previous versions (Libscomb and Hunke 2004). The momentum equation has been modified using scaling arguments to better simulate marginal ice under free drift (Connolley et al. 2004). Salt and freshwater exchange between the sea ice and surrounding ocean are calculated using a nonzero, constant reference salinity of sea ice in CCSM3 (Schmidt et al. 2004). The adoption of a single value of salinity in the sea ice ensures that salt is conserved in the full ocean–ice system.

The albedo parameterization in CCSM3 matches observations of the seasonal dependence of the albedo on snow depth, ice thickness, and temperature within the uncertainty of the measurements in the Arctic and Antarctic (Perovich et al. 2002; Brandt et al. 2005). The dependence on temperature provides a simple mechanism to account for snow wetness and ponding. However, when the ice is covered by cold dry snow, the albedo parameterization in CCSM3 is biased low by about 0.07 compared to observations. The CCSM3 applies a value more appropriate for wet snow rather than dry snow under these conditions. Since the incoming shortwave is too low by about 50 W m^{-2} in May and 90 W m^{-2} in June, the albedo adjustment is necessary to ensure the correct timing for the onset of sea ice melting.

f. Coupling methodology

The physical component models of CCSM3 communicate through the coupler, an executive program that governs the execution and time evolution of the entire system (Craig et al. 2005; Drake et al. 2005). CCSM3 comprises five independent programs, one for each of the physical models and one for the coupler. The physical models execute and communicate via the coupler in a completely asynchronous manner. The coupler links the components by providing flux boundary conditions and, where necessary, physical state information to each model. The coupler monitors and enforces flux conservation for all fluxes that it exchanges among the components. The coupler can exchange flux and state information among components with different grid and time steps. Both of these capabilities are used in the standard configurations of CCSM3. State data is exchanged between different grids using a bilinear interpolation scheme, while fluxes are exchanged using a second-order conservative remapping scheme. The basic state information exchanged by the coupler includes temperature, salinity, velocity, pressure, humidity, and air density at the model interfaces. The basic fluxes include fluxes of momentum, water, heat, and salt across the model interfaces.

In the standard T85 $\times$ 1 configuration, the atmosphere, land, and sea ice exchange fluxes and state information with the coupler every hour, while the ocean exchanges these data once per day. The internal time steps for the land, atmosphere, ocean, and sea ice components are 10 min, 20 min, 1 h, and 1 h, respectively. Special provisions are made in the ocean to approximate the diurnal cycle of insolation (Danabasoglu et al. 2006). During integration, the coupler repeats a sequence of coupling operations. This cycle includes transmission of data to the ocean, land, and sea ice; reception of data from the sea ice and land; transmis-

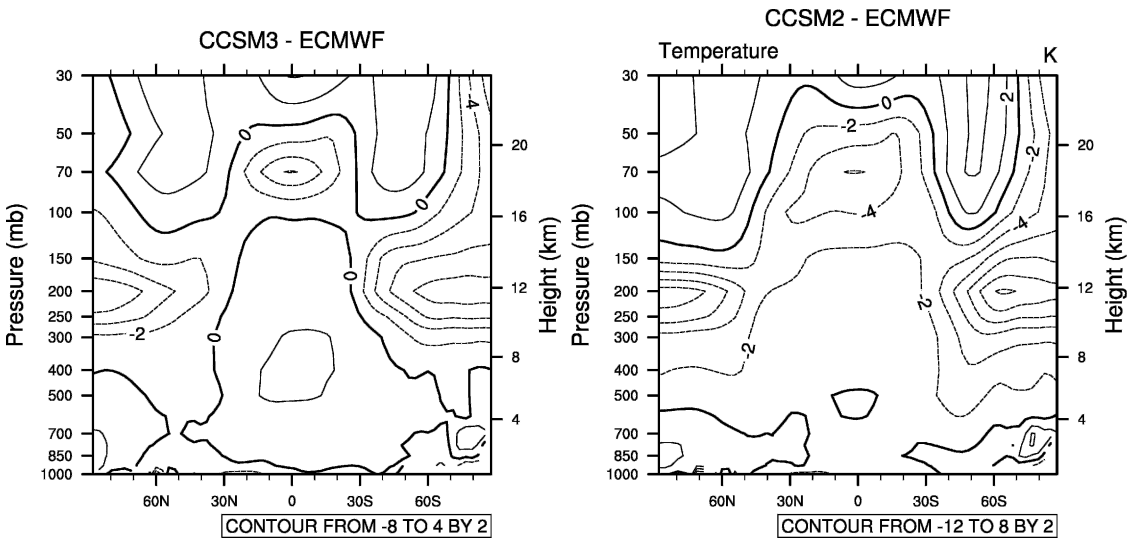

FIG. 1. Differences in the annual-mean, zonally averaged atmospheric temperature profiles between the ECMWF reanalysis (Kållberg et al. 2004) and (left) CCSM3 and (right) CCSM2.

sion to the atmosphere; and finally reception from the ocean and atmosphere.

3. The mean coupled climate

There have been several significant improvements in the climate produced by CCSM3 relative to the climate simulated by CCSM2. These improvements are evident in a comparison of the control integrations of the two models for present-day conditions. In these comparisons, the mean climate produced by CCSM2 is represented by the average of years 900–1000 from its control simulation in its standard T42 × 1 configuration. This time period includes the interval that Kiehl and Gent (2004) used to describe the climate of CCSM2. The mean climate produced by CCSM3 is represented by the average of years 400–500 from a control simulation using the model at its highest standard resolution (T85 × 1; the appendix). This time period is the same interval evaluated by Hurrell et al. (2006). Because of secular drift, the comparison between the two integrations can differ depending upon the choice of time periods used in the analysis (section 4 and Kiehl and Gent 2004). However, the trends are sufficiently small that the differences in the fields examined in this overview of CCSM3 are not appreciably affected. This comparison is also affected by changes in both the physics and the resolution of the atmosphere and land components from CCSM2 to CCSM3. The effects of just changing resolution in these components are discussed by Hack et al. (2006).

a. Thermodynamic and dynamic properties of the atmosphere

The atmospheric temperatures from CCSM3 have improved in two main aspects relative to the simulation with CCSM2 (Fig. 1). First, CCSM2 exhibits a significant cold bias in the temperatures near the tropical tropopause. In the region 30°S–30°N and between 70 and 150 mb, the annual-mean temperature from CCSM2 is 3.9 K colder than the average temperature from the 40-Yr European Centre Medium-Range Weather Forecasts (ECMWF) Re-Analysis (ERA-40; Kållberg et al. 2004). Due primarily to changes in the cloud parameterizations to produce optically thicker cirrus clouds in accordance with observations (Boville et al. 2006), the CCSM3 is warmer in this region by 2.3 K compared to CCSM2. Thus, the tropopause temperatures in CCSM3 are 1.6 K too low relative to the reanalysis. This represents a 60% reduction in the cold temperature bias. Second, the temperatures in both polar atmospheres (150–300 mb) from CCSM2 are significantly colder than meteorological analyses. For the northern polar region between 60° and 90°N and the corresponding southern region between 60° and 90°S, CCSM2 underestimates the annual-mean temperatures by 6.9 and 11.3 K, respectively. The temperatures in CCSM3 increase in these two regions by 2.3 and 3.9 K, respectively. This represents a 33% decrease in the temperature bias in both hemispheres. The CCSM3 is still too cold by 4.6 and 7.4 K in the northern and southern polar regions.

Several aspects of the zonal wind have also improved

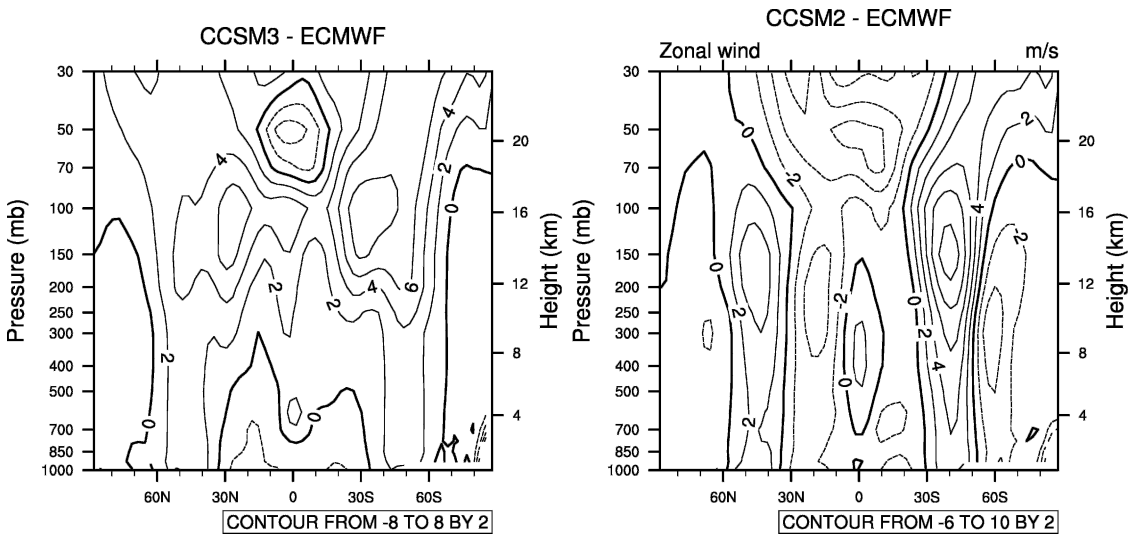

FIG. 2. As in Fig. 1 but for zonal wind speed.

in CCSM3. In CCSM2, the velocities in the westerly jet centered at 200 mb in the Southern Hemisphere are too large by up to 11 m s^{-1} (Fig. 2). In CCSM3, the maximum bias in wind speed in this jet is reduced to approximately 8.5 m s^{-1}. CCSM2 also overestimates the annual-mean easterly velocities in the equatorial atmosphere. The largest biases shown in Fig. 2 occur at roughly 50 mb near the lower edge of the mesospheric jets. In CCSM3, the difference relative to meteorological analyses is reduced by nearly 4 m s^{-1}. However, the tendency of the model to simulate stronger winds in the northern tropospheric jet is somewhat exacerbated in CCSM3.

b. Energy balance at the surface and top of model

The most significant change in the radiation budget of CCSM3 (Table 1) is the disposition of solar radiation in the atmosphere. The atmosphere in CCSM3 absorbs 7.1 W m^{-2} more shortwave radiation under clear-sky conditions and 7.9 W m^{-2} more under all-sky conditions than CCSM2. The increased absorption is caused primarily by the introduction of absorbing aerosol species (section 2b) and the updates to the extinction of near-infrared radiation by water vapor. The new aerosols increase the absorption by 2.8 W m^{-2} for both clear-sky and all-sky conditions. The new treatment of near-infrared extinction by H_2O increases the global-mean clear-sky and all-sky atmospheric absorption by 4.0 and 3.1 W m^{-2}, respectively. The enhanced absorption reduces surface insolation by an equal amount. As a result, the net surface shortwave flux in CCSM3 is 9 W m^{-2} smaller than that in CCSM2 (Fig. 3). The new annual mean insolation of 160 W m^{-2} is consistent with several empirical estimates (Kiehl and Trenberth 1997), although it is lower than the most recent International Satellite Cloud Climatology Project (ISCCP) value of 166 W m^{-2} (Zhang et al. 2004). Despite the improvements in the physics of CCSM3, the changes in insolation in several regions degrade the correspondence with the ISCCP estimates. Some of the largest discrepancies between model and ISCCP calculations occur in the Tropics. Here it is interesting to note that ISCCP overestimates the all-sky downwelling flux by 21 W m^{-2} compared to surface radiometers since the ISCCP calculations do not fully account for the effects of tropical aerosols from biomass burning (Zhang et al. 2004).

The fidelity of the shortwave cloud forcing in CCSM3 has improved relative to estimates from the Earth Radiation Budget Experiment (ERBE) (Harrison et al. 1990; Kiehl and Trenberth 1997), especially in the

TABLE 1. Global annual-mean radiative properties of CCSM2 and CCSM3 (W m^{-2}).

Flux/convergence	CCSM2	CCSM3	Observation
Shortwave atmospheric convergence			
All sky	66.7	74.6	70.9*
Clear sky	62.8	69.9	68.3*
Shortwave cloud forcing	−48.3	−54.0	−54.1**
Shortwave surface net all-sky flux	168.5	159.5	165.9*
Longwave surface net flux			
All sky	65.3	59.4	49.4*
Cear sky	93.6	86.1	78.7*

* ISCCP FD (Zhang et al. 2004).
** ERBE (Harrison et al. 1990; Kiehl and Trenberth 1997).

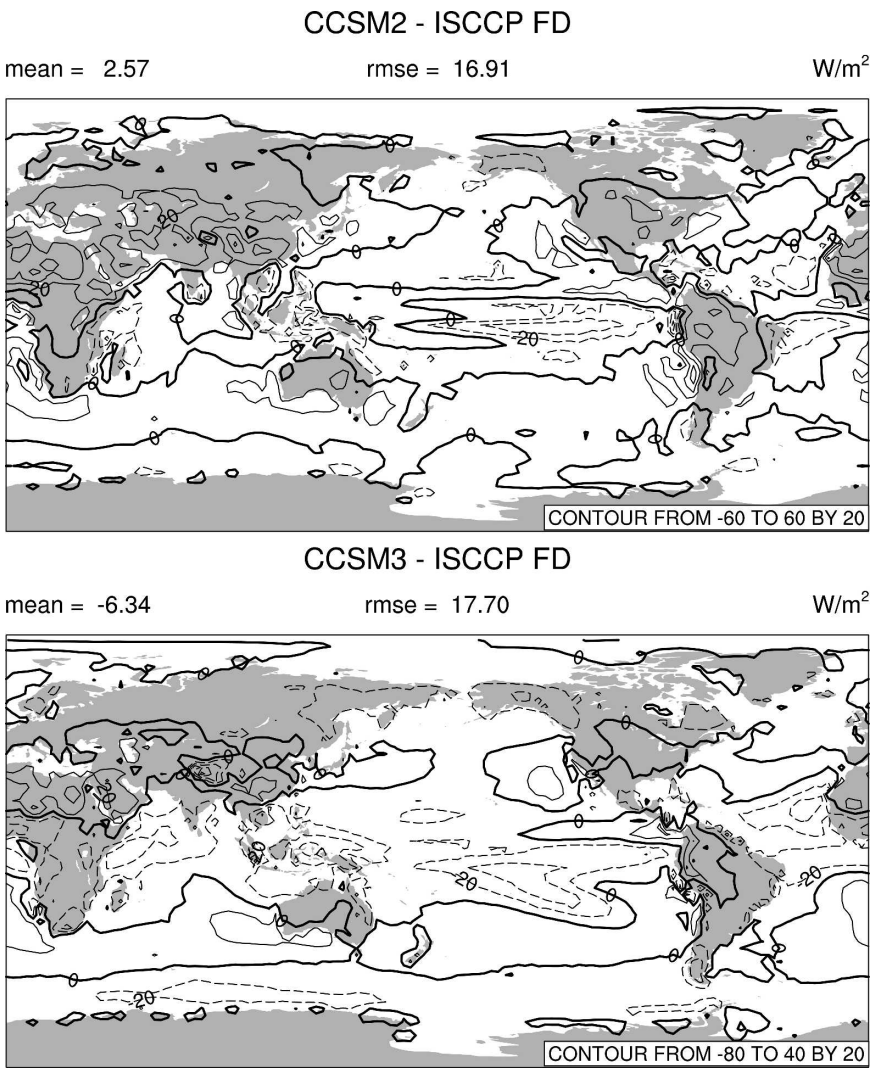

FIG. 3. Differences in annual-mean net surface insolation between the ISCCP FD dataset (Zhang et al. 2004) and (top) CCSM2 and (bottom) CCSM3.

storm tracks (Fig. 4). CCSM2 underestimates the magnitude of global annual-mean shortwave cloud forcing by 5.8 W m^{-2}, while CCSM3 reproduces the ERBE estimates to within 0.1 W m^{-2}. The largest zonal-mean differences occur in the storm track latitudes at 60°N and 60°S and in the tropical latitudes of the ITCZ between 10°N and 10°S. The increased forcing is in better agreement with the satellite data for the storm tracks and in slightly worse agreement for the Tropics.

The global-mean all-sky and clear-sky surface longwave fluxes have decreased by 6.9 and 7.5 W m^{-2} relative to CCSM2. The reductions in clear-sky flux in polar regions are related to the new longwave parameterization for water vapor (Collins et al. 2002a). These changes bring the model into much better agreement with in situ observations (Briegleb and Bromwich 1998).

c. Sea surface temperature and salinity

Several of the systematic errors in SSTs in CCSM2 have been reduced in CCSM3. Earlier versions of CCSM have consistently generated a region of equatorial surface water in the eastern Pacific that is colder than observed and extends too far west into the warm pool. The cold SST bias in the central equatorial Pacific exceeds 2 K in CCSM2, and it is less than 1 K in CCSM3. For CCSM3, the SSTs in this region have increased by between 1 and 2 K in the central and western Pacific (Fig. 5). A substantial fraction of the SST increase is caused by revisions to the treatment of the

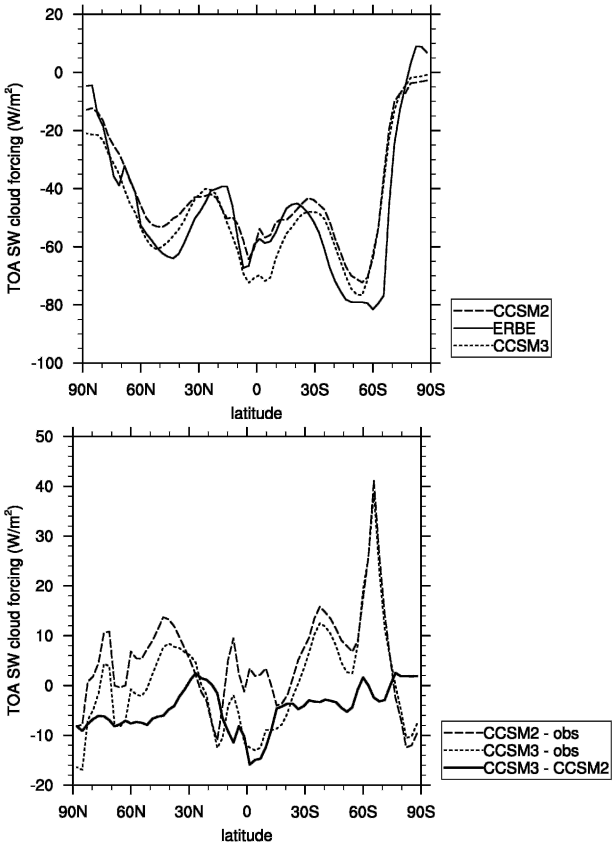

FIG. 4. (top) Annual-mean, zonally averaged shortwave cloud forcing from CCSM2, CCSM3, and ERBE (Harrison et al. 1990; Kiehl and Trenberth 1997) and (bottom) differences among the shortwave forcing estimates.

diurnal cycle of insolation absorbed in the ocean mixed layer (Danabasoglu et al. 2006). In CCSM3, the equatorial SSTs in the warm pool are underestimated by between 0.2 and 0.5 K.

Like CCSM2, the CCSM3 also overestimates the SSTs by as much as 7°C in narrow coastal regions west of Baja and southern California, Peru and Chile, and southwest Africa (section 5d). As discussed in Large and Danabasoglu (2006), surface heat fluxes cannot account for such large biases. Instead, ocean processes such as coastal upwelling appear to be playing an important role in establishing these biases. This is consistent with the insensitivity of the biases to the reduction in solar insolation in these regions from CCSM2 to CCSM3. The SST depends on both the strength and temperature of the upwelling. Therefore, improvements in the alongshore wind component should affect the upwelling strength but may not necessarily have much influence on the SSTs.

The global sea surface salinity is about 0.4 psu too fresh in both CCSM2 and CCSM3, but there are more significant regional differences. In the tropical Indian and Pacific Oceans, CCSM3 rainfall generally exceeds CCSM2 and observational estimates (Fig. 6). Therefore, areas such as the western tropical Pacific warm pool where CCSM2 is too salty are improved in CCSM3, while areas such as the western Indian Ocean and central South Pacific are now much too fresh (Large and Danabasoglu 2006). The reduction in salinity is related to the stronger double ITCZ in CCSM3. The effects of CCSM3 precipitation errors on surface salinity, ocean stratification, and tropical Pacific circulation are further discussed in Large and Danabasoglu (2006).

d. Oceanic heat transport

Figure 7 shows the northward heat transports by the Atlantic and global oceans. As a result of the ~0.3 PW increase in the Atlantic transport by CCSM3 relative to CCSM2 (lower panel), CCSM3 is in agreement with all direct estimates from complete Atlantic transects to within the observational uncertainties (upper panel). This difference is related to a change in the overturning circulation in the North Atlantic, where the maximum below 500-m averages is about 22 Sv in CCSM3 (Bryan et al. 2006) and only about 15 Sv in CCSM2. The global change in heat tranport is less because CCSM3 has less Pacific northward transport than CCSM2 (lower panel). Nonetheless, the agreement with the direct estimates and the partitioning of the transport between basins are both improved (upper panel).

e. Sea ice thickness and concentration

The fidelity of Arctic sea ice thickness and distribution have improved in CCSM3 relative to earlier versions of the model. The annual-mean ice thickness is between 2 and 2.5 m over the central Arctic basin with thicknesses reaching 3–4 m next to the Canadian Archipelago and in the East Siberian Sea (Fig. 8). CCSM3 agrees well with submarine measurements of sea ice thickness from Bourke and Garrett (1987) and Rothrock et al. (1999), although the model is too thin by about 1 m within about 400 km of the Canadian Archipelago and too thick by about 2 m in the East Siberian Sea. The sea ice in CCSM2 is considerably thinner, with ice in the central Arctic averaging about 1.5 m. The increase in the thickness in CCSM3 is due to improvements in the downward longwave radiation in winter.

Improvements in the pattern of sea ice thickness in CCSM3 can be attributed to effects of the increased resolution of the atmosphere on the polar wind field (Fig. 9; DeWeaver and Bitz 2006). In winter the sea ice concentration in the Atlantic sector of the Arctic in CCSM3 is about the same as in CCSM2, with too little ice in the Barents Sea and too much ice in the Labrador

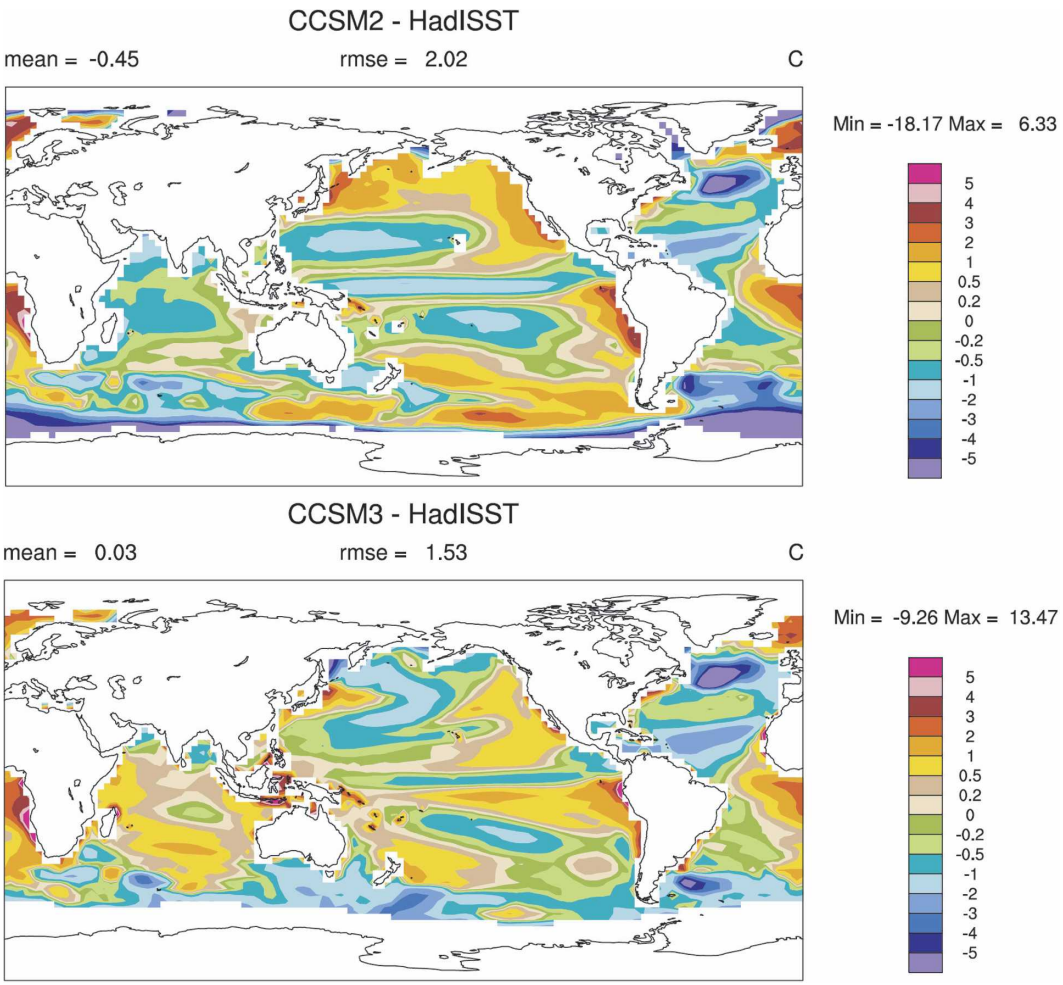

FIG. 5. Differences in annual-mean surface temperature between the HadISST dataset (Rayner et al. 2003) and (top) CCSM2 and (bottom) CCSM3.

Sea. The wintertime ice coverage is now too extensive in the Okhotsk Sea in CCSM3. In the Northern Hemisphere, the mean summertime sea ice coverage agrees well with satellite observations (Holland et al. 2006).

The characteristics of the sea ice in the Southern Hemisphere are described in detail by Holland et al. (2006). The sea ice concentration in CCSM3 is less extensive than in CCSM2 year-round. CCSM3 is still too extensive by about 20% compared with satellite observations of the Southern Ocean (Cavalieri et al. 1997). Ice thickness is much improved in CCSM3 compared to recent observational estimates of Antarctic sea ice (Timmermann et al. 2004).

The CCSM3 model's sea ice described here is from the high-resolution configuration of the model. No changes are made to the sea ice model component for the configurations at lower atmospheric resolution, although the sea ice that is simulated changes considerably. The key difference is that the perennial ice is about 1 m thicker in the moderate resolution configuration than it is at higher resolution. In addition, there is a shift in the thickness pattern mentioned above, and the ice tends to be more extensive. These changes are documented by Holland et al. (2006) and DeWeaver and Bitz (2006).

f. Climate sensitivity

Climate sensitivity is a measure of the change in a climate simulation in response to external forcing. According to its traditional definition, climate sensitivity is the increase in global-average annual-mean surface temperature when the atmospheric concentration of carbon dioxide is doubled. Although climate sensitivity is not a useful metric for regional climate change, it has proved to be a very useful index for categorizing the response of multimodel ensembles to a given climate-change scenario (Houghton et al. 2001).

The equilibrium sensitivity of CCSM3 in its high-

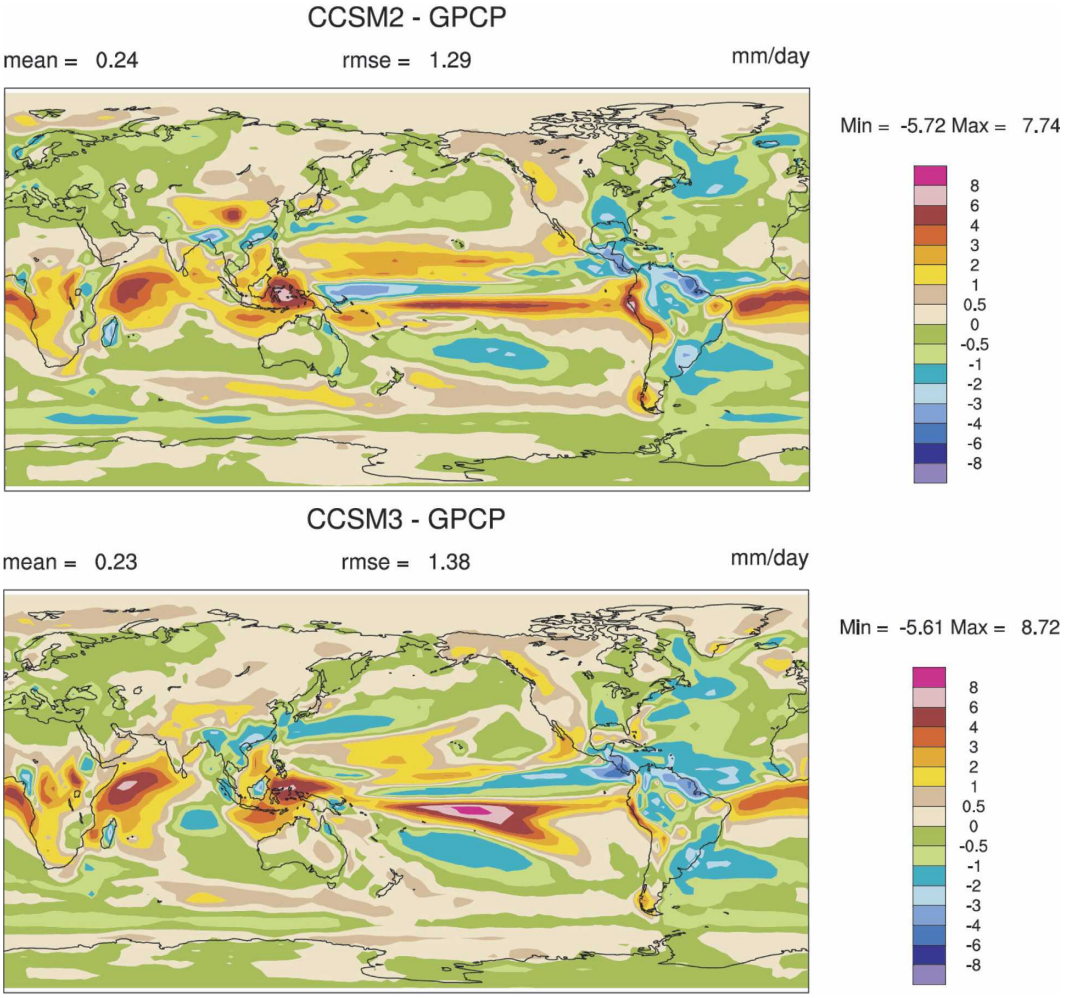

FIG. 6. Differences in annual-mean total surface precipitation between the GPCP dataset (Adler et al. 2003) and (top) CCSM2 and (bottom) CCSM3.

resolution configuration is 2.7 K for doubling CO_2 from 355 to 710 ppmv (Kiehl et al. 2006). This is higher than the equilibrium sensitivity of 2.2 K for CCSM2 and the sensitivity of 2.0 K for CSM1 (Kiehl and Gent 2004). The two factors contributing to the increased sensitivity are the changes in the cloud processes in CAM (section 2b) and the resolution-dependent tuning of the cloud processes (section 2a). The largest differences in cloud response are associated with low clouds. The global-mean low-cloud cover increases in response to higher radiative forcing much less rapidly in CCSM3 than in CCSM2, and the zonal-mean low-cloud cover in CCSM3 actually decreases between 30° and 60°S when concentrations of CO_2 are doubled (Kiehl et al. 2006). In addition, the climate sensitivity of CCSM3 increases with increasing spatial resolution from the T31 × 3 to T85 × 1 configurations. The change in sensitivity is directly related to the variation in low-cloud radiative feedbacks with resolution (Kiehl et al. 2006). The aspects of the cloud parameterizations that cause the low clouds to be particularly sensitive to greater radiative forcing and spatial resolution are still under investigation.

4. Stability and long-term behavior of the coupled integration

CCSM3 has been designed to provide stable simulations relatively free of secular trends under fixed boundary conditions. The stability in the model system is an important design objective for two reasons. First, the absence of large trends is a necessary but not sufficient test of the conservation of energy, mass, and total water content of each of the components. Second, drift-free simulations are required for some of the more demanding applications of the model, including simulations of the carbon cycle that require millennia to

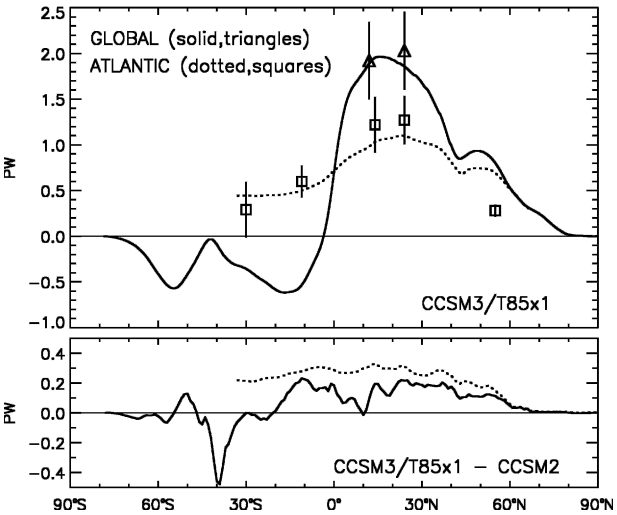

FIG. 7. (top) Northward total transport of heat in the ocean model from integrals across the Atlantic (dotted line) and around the globe (solid line). The model values include the resolved and parameterized eddy components and the isopycnal diffusion. The squares and triangles with accompanying error bars are, respectively, the Atlantic and global results of individual section analyses compiled by Bryden and Imawaki (2001). Uncertainties in the observational estimates are typically ±0.3 PW. Note that the 55°N section did not include the Labrador Sea. (bottom) Differences between the transports of heat in the Atlantic (dotted) and around the globe (solid line) between CCSM3 and CCSM2.

attain equilibrium. The stability can be addressed by examining the energy budget and other properties of an integration for present-day conditions during years 100–600 (appendix).

In order for the climate system to be in equilibrium, the exchange of radiative energy across the top of the atmospheric model (TOM) must be zero. During the initial stages of a climate model integration, it is usually very difficult to achieve a precise time-mean energy balance and, instead, the system gains or loses a small amount of energy during each annual cycle. The exchange of radiant energy is the difference between the net shortwave radiation absorbed by the system and the net longwave radiation emitted by the system. For CCSM3, the annual-mean and rms TOM energy balance is -0.21 ± 0.28 W m^{-2} under present-day conditions (Fig. 10). Since the sign convention on the TOM balance is positive downward, on average the CCSM3 loses energy. This loss rate is nearly identical to the loss rate of -0.2 W m^{-2} for CCSM2 (Kiehl and Gent 2004). Since the annual-mean net solar radiation absorbed at the TOM under all-sky conditions is 234.2 W m^{-2}, the energy imbalance in the system is equivalent to 0.08% of the net solar input. The TOM all-sky and clear-sky fluxes are relatively stable, with trends between -0.01 and -0.03 W m^{-2} century^{-1}.

Similarly, equilibrium of the climate system requires that the global-mean surface energy balance also be identically zero. The (positive downward) exchange of energy among the atmosphere and surface components is the difference between the net downward all-sky shortwave radiation, the net upward all-sky longwave radiation, the latent heat flux including the effects of precipitation, and the sensible heat flux. In the model, the heat storage in soil and the energy used to melt snow are relatively minor compared to the individual terms in the surface energy exchange. For CCSM3, the annual-mean and rms surface energy balance is -0.24 ± 0.21 W m^{-2} (Fig. 10). Detailed diagnostics provided by each component and by the coupler indicate that this imbalance is not caused by a violation of the conservation of energy. The land and ocean model components each supply about half the flux constituting the total surface imbalance. The land component of the surface balance is associated with the heat required to melt snow. The fact that the surface and TOM are losing energy indicates that the model is not in equilibrium even after 600 years of integration. Evidence from long simulations of paleoclimate regimes suggests that the time scale for CCSM3 to approach energetic equilibrium is greater than 2000 yr.

The net energy absorbed by the atmosphere is just the difference between the TOM and surface energy balances. For CCSM3, the mean and rms energy absorbed by the atmosphere is 0.02 ± 0.13 W m^{-2} (Fig. 10). The atmospheric model includes a correction applied at each time step that sets the change in atmospheric energy equal to the globally integrated fluxes exchanged with the surface and top of the model (Collins et al. 2004). The atmospheric energy is approximated as the sum of the total potential energy and the lateral kinetic energy. The correction is introduced as a vertically uniform adjustment to the atmospheric temperatures. In the absence of that correction, the time-mean global-average energy lost by the atmosphere is -0.27 W m^{-2}. This residual loss is due primarily to temperature diffusion and secondarily to numerical approximations.

Since the simulated climate system is slowly losing energy, the global mean surface temperature should decrease slowly with time. By the end of the first century, the area of Arctic sea ice has settled into an oscillation about its long-term mean value. After this initial 100-yr period, the surface temperature decreases by -0.011 K century^{-1}. Most of this trend is manifested in the Southern Hemisphere between 30° and 90°S, which cools at a rate of -0.04 K century^{-1}. The temperatures in the Tropics between 30°S and 30°N and the Northern Hemisphere between 30° and 90°N increase by less

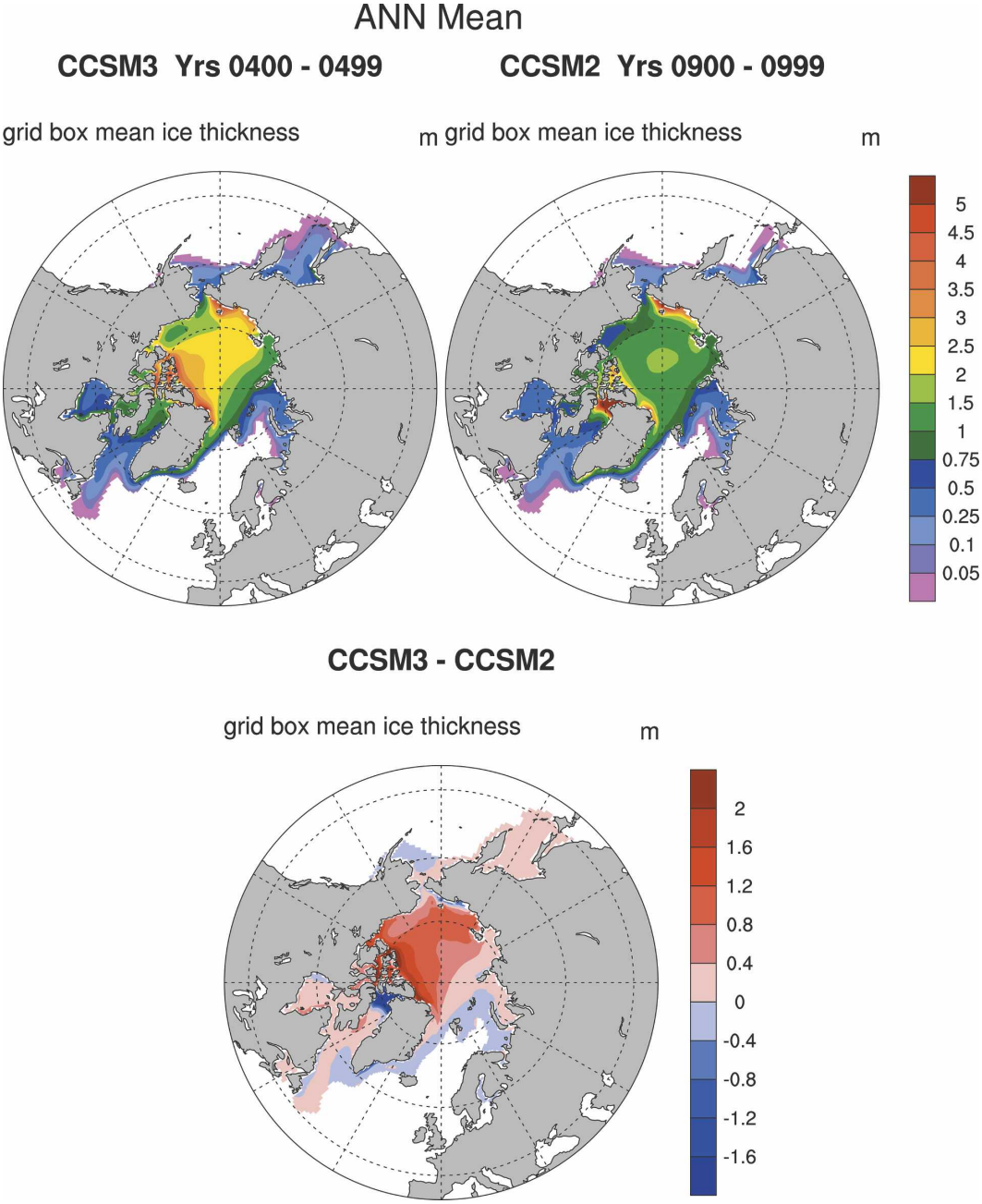

FIG. 8. Annual-mean sea ice thickness in the Northern Hemisphere from (top left) CCSM3, (top right) CCSM2, and (bottom) the difference between CCSM3 and CCSM2.

than 2×10^{-4} K century^{-1}. The trend in the global volume-mean ocean temperature is -0.05 K century^{-1}. As in CSM1 (Boville and Gent 1998), the initial ocean adjustment to the energy imbalances at the ocean surface occurs well below the mixed layer (Fig. 11).

The decrease in the temperature of the Southern Hemisphere can be explained either by the expansion of the southern sea ice extent or by the persistent cooling of the deep ocean water upwelling adjacent to Antarctica. The trends in sea ice in the Northern and Southern Hemispheres are -0.02×10^6 and 0.18×10^6 km^2 century^{-1}, respectively (Fig. 12). These changes correspond to changes in ice concentration (expressed in fractional area) of -0.002% and 0.015% century^{-1}. The temperature trend can be decomposed into a sum of terms associated with the trends in the areas and temperatures of the Southern Ocean, southern sea ice, and ice over Antarctica. The decomposition shows that

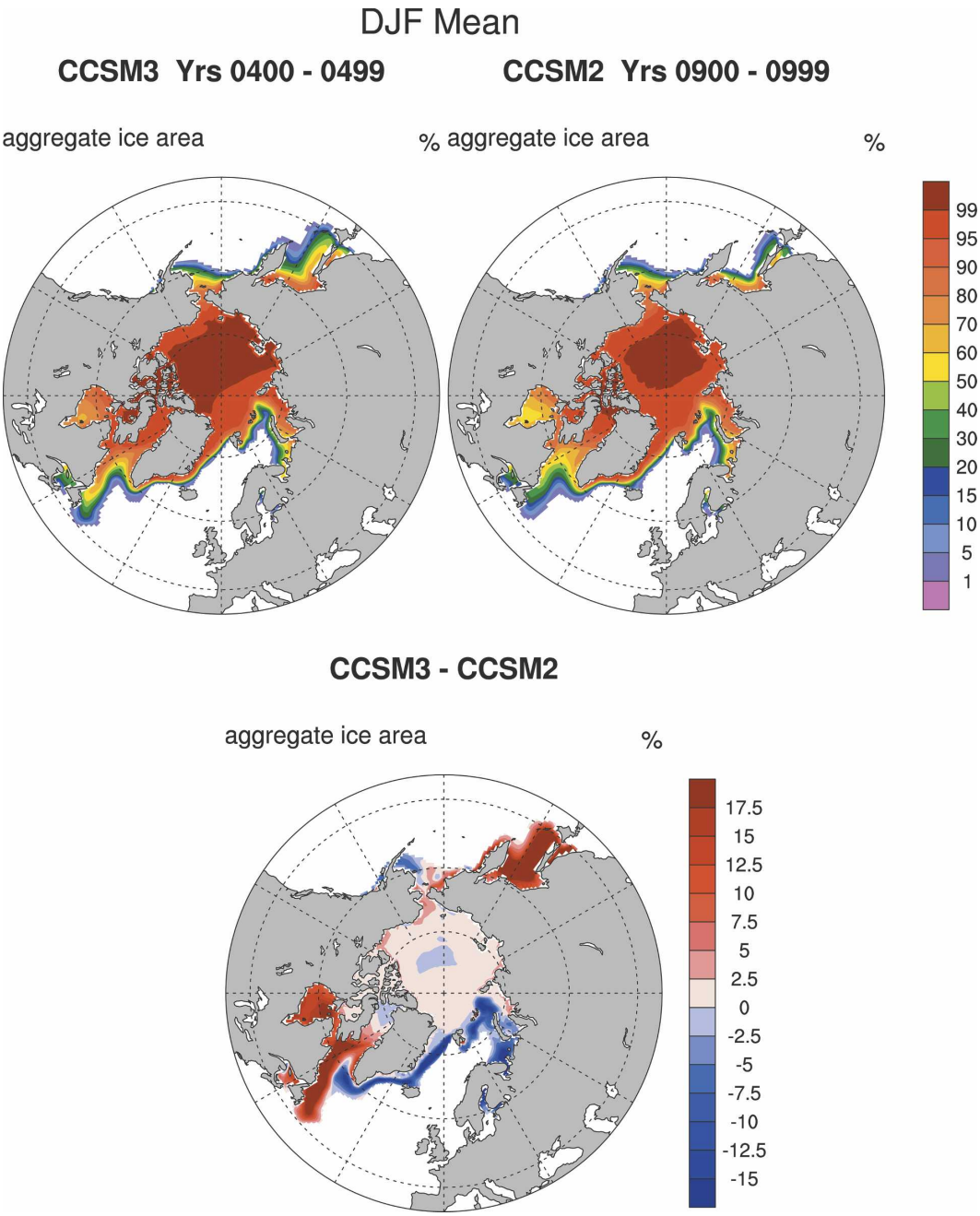

FIG. 9. As in Fig. 8 but for the DJF-mean sea ice area in the Northern Hemisphere.

83% of the Southern Hemisphere trend is determined by the combination of the upward trend in sea ice area and the −18.6-K average temperature differential between the sea ice and surrounding ocean.

The trend in the global volume-mean salinity is -6.2×10^{-5} psu century^{-1} (Fig. 11). Compared to the global mean salinity of 34.72 psu, the trend in salinity is equivalent to a relative change of -2×10^{-4}% century^{-1}. This reduction in salinity is caused by the adjustment of the soil moisture in the deepest layers of the land model during the first 300 years of integration (Kiehl and Gent 2004). Excess deep soil moisture is gradually released to the oceans by river runoff. These trends are smaller in magnitude, but opposite in sign, to the changes in salinity in CCSM2 (Kiehl and Gent 2004).

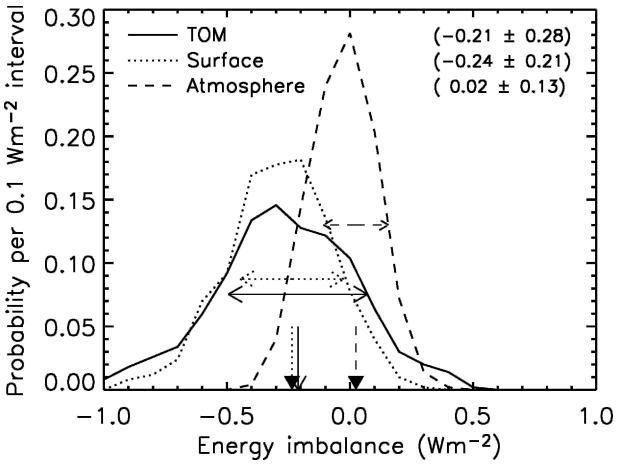

FIG. 10. Probabilities of annual-mean energy imbalances in CCSM3 at the top of the model (TOM), the surface, and in the atmosphere. The probabilities are obtained from years 100 through 600 of the control integration. Vertical arrows represent series-mean imbalances, and horizontal arrows represent the 2σ range of annual imbalances. (top to bottom) Values in the upper right are the mean and 1σ imbalances for the TOM, surface, and atmosphere.

5. Challenges for further development

While many features of the climate are simulated with greater fidelity by CCSM3 than CCSM2, there are still significant biases that should be addressed in future generations of CCSM. These systematic errors can be illustrated by comparing the CCSM3 control integration against observations and meteorological analyses for the present-day climate.

a. Representation of major modes of variability

The basic characteristics of the ENSO episodes simulated by CCSM2 and CCSM3 are quite similar. Two of the most important properties are the total variance and power spectrum of SST anomalies in the central Pacific. The results for the Niño-3.4 region (5°S–5°N, 120°–170°W) are representative of other regions in the tropical Pacific.

The meteorological reanalysis by Kistler et al. (2001) for 1951–2000 provides the observed properties for this region. The reanalysis represents a relatively short data record compared to the length of the CCSM2 and

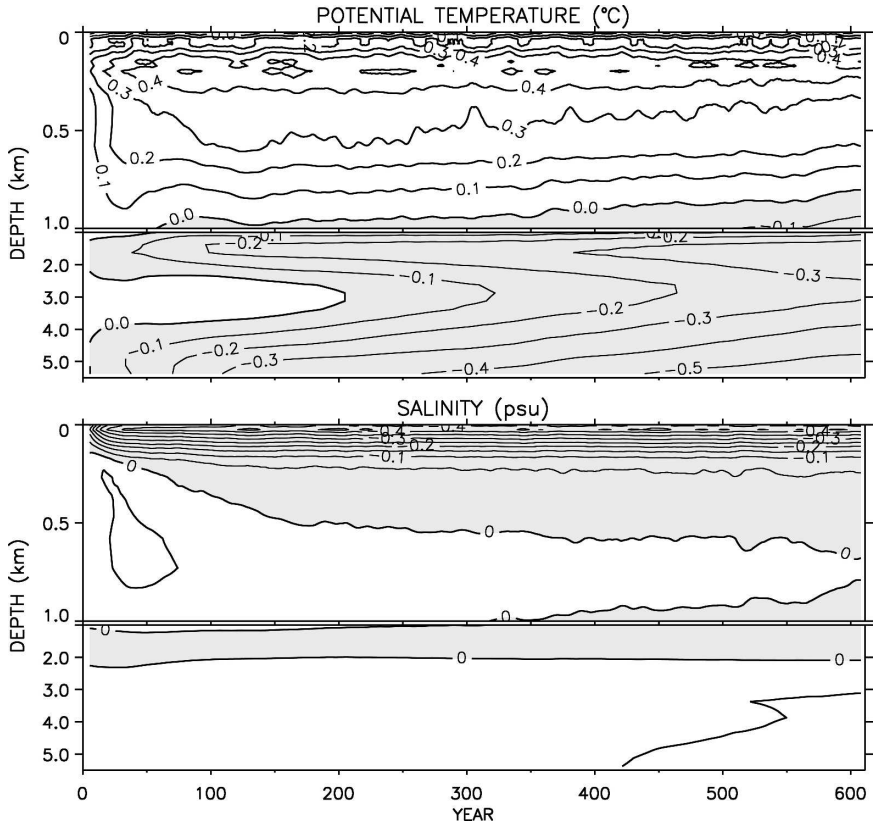

FIG. 11. Difference between simulated global-mean ocean (top) potential temperature and (bottom) salinity and the observed climatological profile (Levitus et al. 1998) as a function of depth and year of simulation.

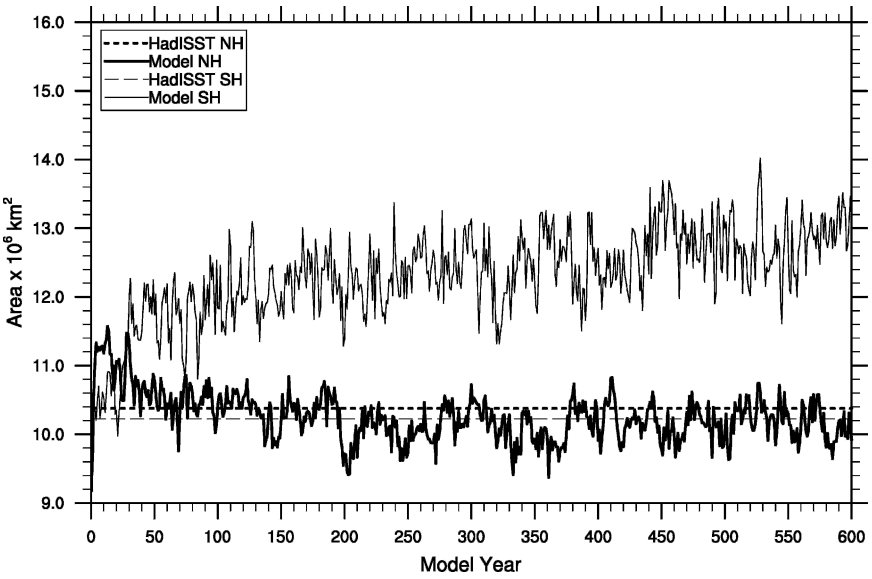

FIG. 12. Annual-mean area of sea ice from the CCSM3 control integration in the Northern Hemisphere (bold lines) and Southern Hemisphere. Observational estimates from the HadISST dataset (Rayner et al. 2003) are shown by dashed lines for each hemisphere.

CCSM3 control runs. In addition, the variance simulated for the Niño-3.4 region in CCSM2 and CCSM3 can change considerably on time scales of 50 yr. For these reasons, the control runs for CCSM2 and CCSM3 are divided into 50-yr segments. The variance and power spectra for each segment are determined separately and then aggregated for comparison against the meteorological reanalysis. The model data used for this purpose includes 650 years of the CCSM2 control integration and 500 years of the CCSM3 integration. The Niño-3.4 temperature anomalies are smoothed using a running 5-month boxcar average before analysis.

The total variance for the smoothed monthly anomalies in the Niño-3.4 temperature for the analysis is 0.78 K, and the mean variances for the 50-yr segments of CCSM2 and CCSM3 are 0.81 and 0.73 K. These results show that the CCSM2 tends to overestimate and the CCSM3 tends to underestimate the variability in the observed record. Approximately 70% of the 50-yr segments from CCSM2 and 40% of the segments from CCSM3 have greater variability than observed. The power spectra of the monthly SST anomalies for the low and intermediate resolutions of CCSM3 are discussed in detail in Yeager et al. (2006). The power spectra for the high-resolution (T85 $\times$ 1) configuration of CCSM3 are compared against the spectra for CCSM2 and the National Centers for Environmental Prediction (NCEP) reanalysis in Fig. 13. The observed ENSOs have a relatively broad spectrum spanning 3–5 yr. The CCSM3, like CCSM2, tends to produce ENSOs with a periodicity of approximately 2 yr. In fact, the spectra of CCSM3 are even more strongly peaked at periods of 2 yr than those of CCSM2, and the variance at periods of 5 yr is smaller and hence less realistic in CCSM3 than in CCSM2.

b. Double ITCZ in the Pacific

Like previous generations of this model, CCSM3 produces a double ITCZ in the tropical Pacific. The

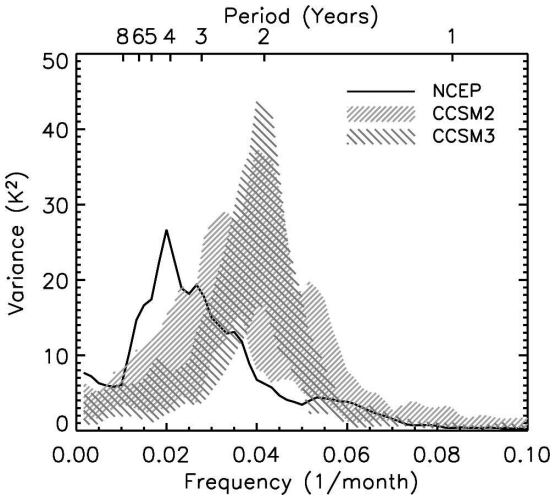

FIG. 13. Power spectra of the monthly Niño-3.4 anomalies for CCSM2, CCSM3, and the NCEP reanalysis (thick line) (Kistler et al. 2001). The range of variance spanned by the spectra of individual 50-yr segments are shown for CCSM2 (light hatching) and CCSM3 (dark hatching).

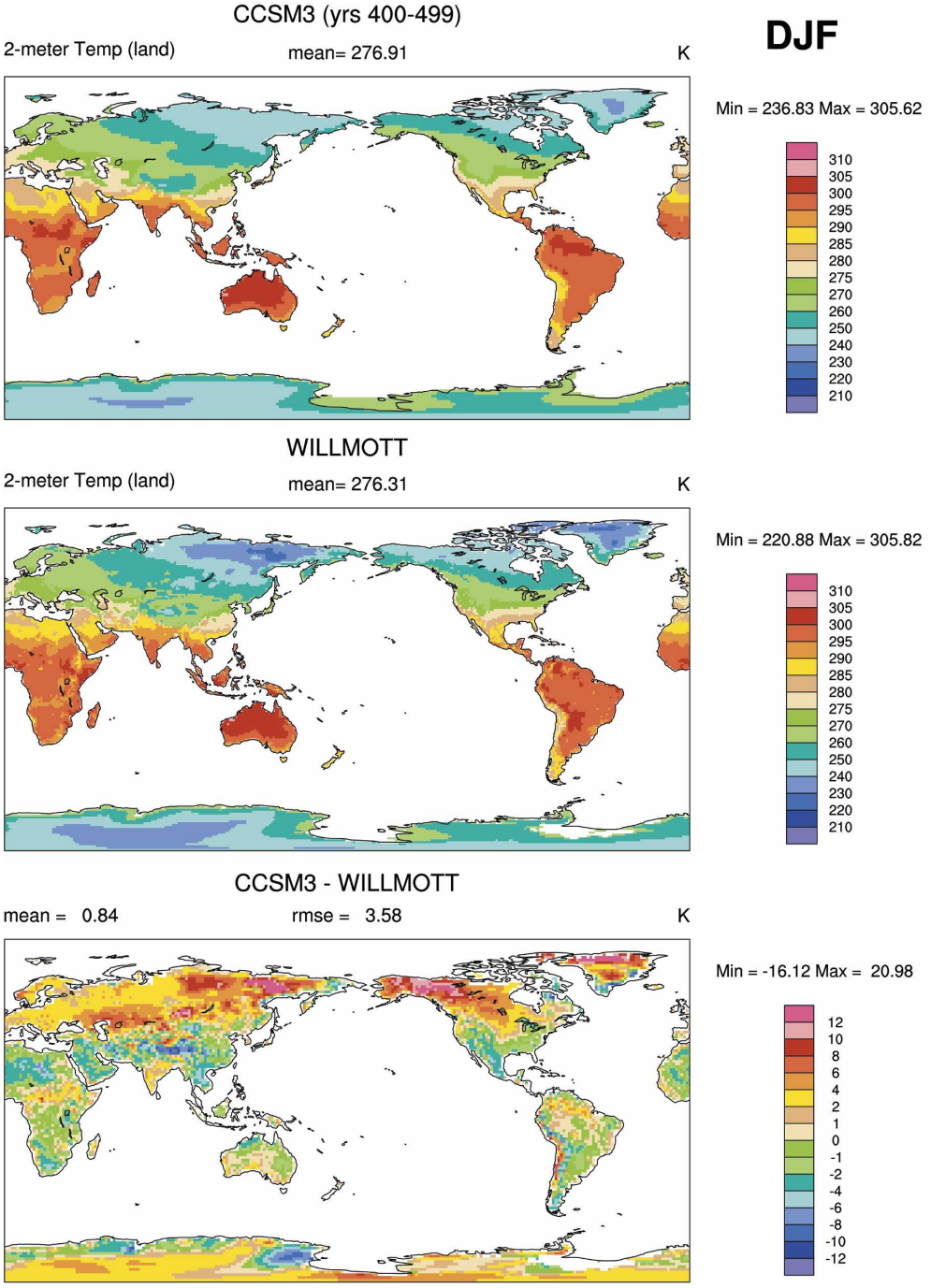

FIG. 14. DJF-mean 2-m surface temperature from (top) CCSM3, (middle) the Willmott and Matsuura (2000) dataset, and (bottom) the difference between CCSM3 and the Willmott estimates.

South Pacific convergence zone (SPCZ) in the observations extends southeastward from the tropical warm pool into the central South Pacific (Fig. 6). In CCSM3, the SPCZ is replaced by a southern branch of the ITCZ that is nearly zonal in orientation. The error is particularly evident during June–August when the real SPCZ is much weaker and less extensive than the modeled convection south of the equator. The model overestimates the local precipitation rate in both branches of the ITCZ by up to 10 mm day^{-1}. The maximum precipitation in the northern half of the warm pool is too intense and is displaced westward by approximately 30°

TABLE 2. Model precipitation for continental regions.

Region	Region box	Precipitation (mm day^{-1})	Error* (mm day^{-1})	Percent error*
Southeast United States	30°–40°N, 80°–100°W	2.4	−0.75	−24
Amazonia	10°S–10°N, 60°–80°W	4.5	−1.7	−28
Southeast Asia	10°–30°N, 80°–110°E	3.1	−1.0	−24

* Error is computed relative to the Willmott and Matsuura (2000) dataset.

relative to the observed maximum. The excess rainfall indicates that the model produces an overly vigorous hydrological cycle for the tropical Pacific Ocean. It also adversely affects the meridional structure of the equatorial Pacific undercurrent (Large and Danabasoglu 2006).

c. *Biases in continental precipitation and temperature*

Although the temperature errors in CCSM3 are smaller than those in CCSM2, there are still large biases in the 2-m air temperatures for sub-Arctic continental regions during boreal winter. The temperatures relative to observations (Willmott and Matsuura 2000) during December–February (DJF) are overestimated by as much as 10 K in parts of Alaska and northern Eurasia (Fig. 14). The mean and rms overestimates for sub-Arctic continental regions north of 50°N during DJF are $+3.9 \pm 5.7$ K. The magnitude of the local errors are generally smaller than those in CCSM2 (Kiehl and Gent 2004). In addition, there are significant deficits in precipitation in the southeast United Sates, Amazonia, and Southeast Asia throughout the annual cycle (Fig. 6). The biases in annual-mean precipitation for these three regions are listed in Table 2. The underestimation of rainfall ranges between 24% and 28% for these areas.

These biases cause dynamic models of vegetation to produce unrealistic distributions of plant functional types in the affected regions (Bonan and Levis 2006). CCSM3 includes a dynamic vegetation module (Levis et al. 2004), but it is not active by default. Models of the terrestrial carbon cycle are very sensitive to both temperature and precipitation. It is difficult to predict the net effect on CO_2 concentrations from biases in these fields because of the multitude of ecological and biogeochemical processes affected. Carbon uptake during photosynthesis, carbon loss during respiration, and vegetation geography depend on temperature and precipitation. In addition, the sensitivity of these processes differs among types of vegetation. Therefore, when there are biases in both temperature and precipitation, it may be difficult to predict the sign of the change in atmospheric CO_2. For these reasons, it will be important to reduce these biases in future versions of CCSM that include biogeochemistry. One option to reduce the positive temperature biases during boreal winter is to use a relationship between snow albedo and equivalent water depth that is more consistent with satellite observations (Oleson et al. 2003).

d. *SST biases and related atmospheric issues in western coastal regions*

CCSM3 produces sea surface temperatures for the western coastal regions that are warmer than observed (Fig. 5). Experiments with prototypes of the coupled model suggest that the biases in SSTs can be caused by underestimates of surface stress parallel to the coast and by overestimates of surface insolation (Large and Danabasoglu 2006). The weaker surface stress results in weaker cooling of the ocean mixed layer, and the excess insolation results in too much solar heating of the upper ocean. These experiments also show that the biases in these areas affect the SST and precipitation over large portions of the Atlantic and Pacific basins. Two examples of the positive SST biases occur in the oceans adjacent to southern Africa and South America. The CCSM3 is compared in Table 3 against observations and analyses for these two western coastal regions av-

TABLE 3. Properties of western coastal ocean regions.

Region	Source	SST (°C)	Stress (N m^{-2})	$S^q_{\downarrow}$ (W m^{-2})	$S^q_{\downarrow,c}$ (W m^{-2})
Africa[b]	Observed[c]	21.7	0.052	221.0	290.1
	CCSM3	25.2	0.051	215.6	286.9
South America[b]	Observed[c]	19.7	0.045	212.5	288.0
	CCSM3	21.5	0.039	208.9	285.7

[a] Flux $S_{\downarrow}$ and $S_{\downarrow,c}$ denote the downwelling surface shortwave flux for all-sky and clear-sky conditions, respectively.

[b] The biases are computed within 15° longitude of the western coasts of Africa (between 30°S and 0°) and South America (between 40°S and 0°). The stress is the magnitude of the alongshore component.

[c] Observed SST is from the HadISST dataset (Rayner et al. 2003), surface stress is from the NCEP reanalysis (Kistler et al. 2001), and surface insolation is from the ISCCP FD dataset (Zhang et al. 2004).

eraged over the annual cycle. In the coastal region adjacent to South America, CCSM3 overestimates the SST by 1.8°C. While earlier generations of CCSM overestimated the surface insolation off South America by more than 50 W m^{-2} in the annual mean, CCSM3 tends to slightly underestimate the surface shortwave flux. The much smaller error in insolation results from several modifications to the cloud parameterizations introduced in CCSM3 (Boville et al. 2006) partly to address this issue. The observational comparison suggests that the alongshore surface stress in CCSM3 may still be too weak, and this may partially explain the 1.8°C error in SST. It should be noted that the surface stress produced by CCSM3 is stronger than that in CCSM2 by up to 0.1 N m^{-2}, partly because of the increased resolution in the atmosphere (Hack et al. 2006). In the case of Africa, CCSM3 underestimates the SST by 3.5°C even though it produces a realistic alongshore stress and slightly underestimates the surface insolation. The effects of other physical processes, including ocean upwelling, on the SST biases are examined further in Large and Danabasoglu (2006).

e. The semiannual SST cycle in the eastern Pacific

CCSM3 produces a fairly strong semiannual cycle for SST in the eastern tropical Pacific that does not occur in the real climate system (Large and Danabasoglu 2006). The region where this discrepancy is particularly evident lies between 5°N–5°S and 110°–90°W. An observational climatology for the seasonal cycle in SST for this region can be derived from the Hadley Centre's sea surface temperature dataset (HadISST) (Rayner et al. 2003). The annual and regional mean temperature from CCSM3 is 25.5°C, and this compares well with the HadISST estimate of 25.2°C. However, the simulated and observed seasonal cycles in the regional mean SST are quite different. The CCSM3-simulated annual cycle has a sine-wave amplitude roughly half that observed and is phased 1.4 months late, while the sine-wave amplitude of the semiannual cycle is roughly twice that observed. The causes for these systematic biases in the model physics have not yet been identified.

f. Underestimation of downwelling shortwave radiation in the Arctic

In the Arctic, CCSM3 underestimates the downwelling all-sky shortwave radiation at the surface throughout the annual cycle. The insolation is underestimated relative to in situ observations from the Surface Heat Budget of the Arctic (SHEBA) experiment (Persson et al. 2002) and to estimates from ISCCP (Fig. 15; Zhang et al. 2004). For this comparison, the ISCCP data from 1984 to 2000 has been averaged to produce a climatology. Between 70° and 90°N, the annual-mean downwelling shortwave fluxes for all-sky conditions are 91 W m^{-2} from ISCCP and 78 W m^{-2} from CCSM3. The corresponding annual-mean clear-sky fluxes differ by only −3.9 W m^{-2}, or −3%. The fluxes during the JJA season are 214 W m^{-2} from ISCCP and 169 W m^{-2} from CCSM3. The corresponding JJA-mean clear-sky fluxes differ by only 8.5 W m^{-2}, or 2.7%. Since the clear-sky fluxes are in good agreement, the underestimate of surface insolation by CCSM3 is caused by an overestimate of the surface shortwave cloud radiative forcing. It should be noted that the excessive cloudiness in winter produces an overestimate of downwelling longwave surface flux by 20 W m^{-2} for December through April. The overestimation of longwave flux partly compensates the underestimation of shortwave insolation in the total surface radiation budget. Further analysis will be required to identify the sources of these errors in the modeled cloud amount, cloud condensate path, and cloud microphysical properties.

6. Summary

A new version of the Community Climate System Model, version 3 (CCSM3), has been developed and released to the climate community. The improvements in the functionality include the flexibility to simulate climate over a wide range of spatial resolutions with greater fidelity. This paper documents the high-resolution (T85 × 1) version used for international assessments of climate change. The atmosphere and land share a grid for the Eulerian spectral atmospheric dynamics running at T85 truncation. The ocean and sea ice share a nominal 1° grid with a displaced pole in the Northern Hemisphere.

The atmosphere incorporates new treatments of cloud and ice-phase processes; new dynamical frameworks suitable for modeling atmospheric chemistry; improved parameterizations of the interactions among water vapor, solar radiation, and terrestrial thermal radiation; and a new treatment of the effects of aerosols on solar radiation. The land model includes improvements in land surface physics to reduce temperature biases and new capabilities to enable simulation of dynamic vegetation and the terrestrial carbon cycle. The ocean model has been enhanced with new infrastructure for studying vertical mixing, a more realistic treatment of shortwave absorption by chlorophyll, and improvements to the representation of the ocean mixed layer. The sea ice model includes improved schemes for the horizontal advection of sea ice and for the exchange of salt with the surrounding ocean. The software has

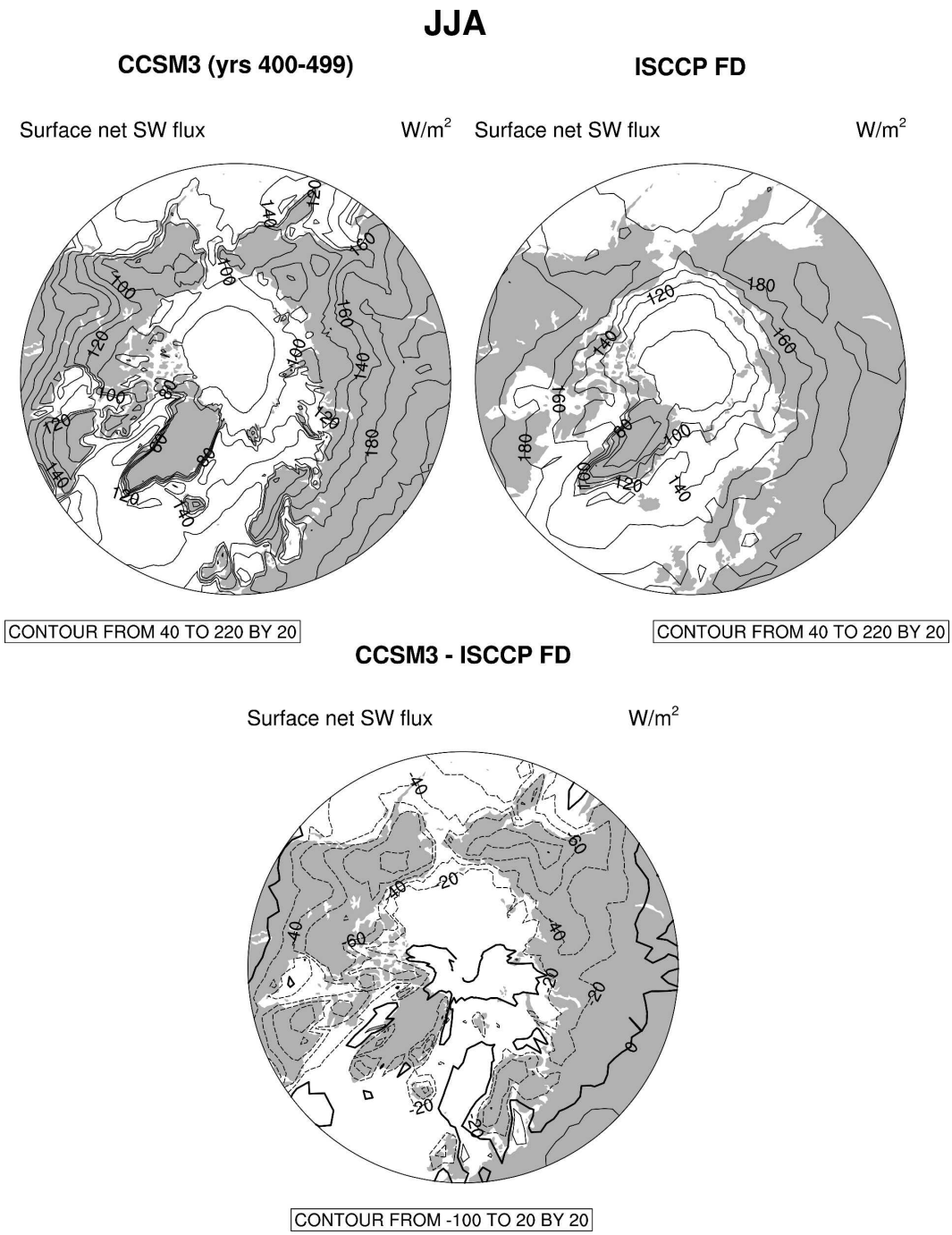

FIG. 15. JJA-mean all-sky net surface shortwave flux from (top left) CCSM3, (top right) the ISCCP FD dataset (Zhang et al. 2004), and (bottom) the difference between CCSM3 and ISCCP.

been designed so that CCSM3 is readily portable to a wide variety of computer architectures.

The climate produced by the high-resolution CCSM3 shows several significant improvements over the climates produced by previous generations of the model. These include reduced sub-Arctic surface temperature biases during boreal winter, reduced tropical SST biases in the Pacific, and more realistic meridional ocean heat transport. The new atmosphere features improved simulation of cloud radiative effects in the storm tracks and during ENSO events (section 3b), smaller biases in upper tropical tropospheric temperatures, and a more realistic surface radiation budget under clear-sky conditions (Collins et al. 2006a). The sea ice features a

TABLE A1. Control integrations using CCSM3.

Resolution	Present (yr)	1%(CO_2) yr^{-1} (yr)	2 × CO_2 (yr)	4 × CO_2 (yr)	1780 (yr)	1870 (yr)	Twentieth century (yr)
T85 × 1	b30.009 (661)	b30.026 (161)	b30.026a (152)	b30.026b (153)	— (0)	b30.020 (235)	b30.030 (8 × 130)
T42 × 1	b30.004 (1001)	b30.025 (214)	b30.025a (301)	b30.025b (301)	b30.100 (499)	b30.043 (302)	— (0)
T31 × 3	b30.031 (748)	b30.032 (171)	b30.032a (157)	b30.032b (160)	b30.105 (433)	b30.048 (154)	— (0)

much more realistic simulation of the spatial distribution of ice concentration and of ice thickness. The climate is stable over at least 700 years subject to perpetual present-day boundary conditions.

There are several aspects that should be improved in future versions of CCSM. These include the periodicity and total variance of ENSO, the double ITCZ in the tropical oceans, and the large precipitation biases in the western tropical ocean basins. Other major modes of variability that are not well-simulated include the Madden–Julian oscillation (Collins et al. 2006a). The errors in continental precipitation and temperatures need to be addressed to facilitate modeling of dynamic vegetation and the terrestrial carbon cycle. While the representation of the surface fluxes in coastal regions west of Africa and South America has improved, there are still significant biases in the coastal SSTs (Large and Danabasoglu 2006). Reduction in these biases will affect the simulation over large areas of the Pacific and Atlantic basins. Finally, there are still significant errors in the radiative energy budget of polar regions. These affect both the seasonal cycle and the climate feedbacks of sea ice.

Research is under way to diagnose these biases at the process level and to test improvements in the physics and dynamics that would enhance the simulation fidelity. At the same time, the model is being extended to include a comprehensive treatment of terrestrial and oceanic biogeochemistry and ecosystem dynamics. Detailed representations of reactive chemistry, photochemistry, and aerosol microphysics have been added to the atmosphere. These developments are the initial steps toward building a more comprehensive model of the entire Earth System that can be applied to climates of the past, present, and future.

Acknowledgments. The authors wish to acknowledge members of the CCSM Software Engineering Group and NCAR's Divisions for Climate and Global Dynamics, Atmospheric Chemistry, and Scientific Computing for their substantial contributions to the development of CCSM3. The suggestions by two anonymous reviewers have helped considerably to improve this description of CCSM3.

The new model would not exist without the significant input and effort from many members of the CCSM working groups. We would like to acknowledge the substantial contributions to and support for the CCSM project from the National Science Foundation (NSF), the Department of Energy (DOE), the National Oceanic and Atmospheric Administration, and the National Aeronautics and Space Administration.

This study is based on model integrations performed by NCAR and the Central Research Institute of the Electric Power Industry (CRIEPI) with support and facilities provided by NSF, DOE, the Ministry of Education, Culture, Sports, Science and Technology (MEXT), and the Earth Simulator Center/Japan Agency for Marine-Earth Science and Technology ESC/JAMSTEC.

We appreciate the financial support from NSF for this special issue of the *Journal of Climate* on CCSM3.

APPENDIX

Control Integrations of CCSM3

A comprehensive suite of control experiments have been performed with CCSM3. The output from these experiments has been released to the climate community and may be readily obtained from the CCSM Web site (online at http://www.ccsm.ucar.edu/models). Most of the experiments have been integrated using each of the three standard configurations of CCSM (section 2a). The experiments include simulations under constant present-day and preindustrial conditions corresponding to 1780 and 1870. To characterize the sensitivity of the model to increased atmospheric concentrations of CO_2, the model has been integrated with a 1% yr^{-1} increase in CO_2 starting from initial conditions obtained from the present-day run. Two other simulations have been branched from the transient 1%(CO_2)

yr^{-1} simulation when the decadal-mean CO_2 concentration is equal to 2 and 4 times its present-day value. The CO_2 concentration is held fixed in each of these runs to the values at the branch points from the transient simulation. For the purposes of these control experiments, the present-day global-mean annually averaged mixing ratio of CO_2 is equal to 355 ppmv, its value in 1990.

The control integrations are shown in Table A1. The table lists the types of experiments, the resolution used in each integration, the length of each experiment in years, and the series identifier for each simulation. More details regarding the types of model output available and the methods for access to these data are available from the CCSM Web site. The control experiment discussed in this paper is b30.009.

REFERENCES

Adler, R. F., and Coauthors, 2003: The version-2 Global Precipitation Climatology Project (GPCP) monthly precipitation analysis (1979–present). *J. Hydrometeor.,* **4,** 1147–1167.

Alexander, M., and Coauthors, 2006: Extratropical atmosphere–ocean variability in CCSM3. *J. Climate,* **19,** 2496–2525.

Ammann, C. M., G. A. Meehl, W. M. Washington, and C. S. Zender, 2003: A monthly and latitudinally varying volcanic forcing dataset in simulations of 20th century climate. *Geophys. Res. Lett.,* **30,** 1657, doi:10.1029/2003GL016875.

Barth, M. C., P. J. Rasch, J. T. Kiehl, C. M. Benkovitz, and S. E. Schwartz, 2000: Sulfur chemistry in the National Center for Atmospheric Research Community Climate Model: Description, evaluation, features and sensitivity to aqueous chemistry. *J. Geophys. Res.,* **105,** 1387–1415.

Bonan, G. B., and S. Levis, 2006: Evaluating aspects of the Community Land and Atmosphere Models (CLM3 and CAM) using a dynamic global vegetation model. *J. Climate,* **19,** 2290–2301.

——, ——, L. Kergoat, and K. W. Oleson, 2001: Landscapes as patches of plant functional types: An integrating approach for climate and ecosystem models. *Global Biogeochem. Cycles,* **16,** 5.1–5.23.

Bourke, R. H., and R. P. Garrett, 1987: Sea ice thickness distribution in the Arctic Ocean. *Cold Reg. Sci. Technol.,* **13,** 259–280.

Boville, B. A., and P. R. Gent, 1998: The NCAR Climate System Model, version one. *J. Climate,* **11,** 1115–1130.

——, P. J. Rasch, J. J. Hack, and J. R. McCaa, 2006: Representation of clouds and precipitation processes in the Community Atmosphere Model (CAM3). *J. Climate,* **19,** 2184–2198.

Brandt, R. E., S. G. Warren, T. C. Grenfell, and A. P. Worby, 2005: Surface albedo of the Antarctic sea ice zone. *J. Climate,* **18,** 3606–3622.

Briegleb, B. P., and D. H. Bromwich, 1998: Polar radiation budgets of the NCAR CCM3. *J. Climate,* **11,** 1246–1269.

——, C. M. Bitz, E. C. Hunke, W. H. Lipscomb, M. M. Holland, J. L. Schramm, and R. E. Moritz, 2004: Scientific description of the sea ice component in the Community Climate System Model, Version Three. Tech. Rep. NCAR/TN-463+STR, National Center for Atmospheric Research, Boulder, CO, 78 pp.

Bryan, F. O., G. Danabasoglu, N. Nakashiki, Y. Yoshida, D.-H. Kim, J. Tsutsui, and S. C. Doney, 2006: Response of North Atlantic thermohaline circulation and ventilation to increasing carbon dioxide in CCSM3. *J. Climate,* **19,** 2382–2397.

Bryden, H., and S. Imawaki, 2001: Ocean heat transport. *Ocean Circulation and Climate,* G. Siedler, J. Church, and J. Gould, Eds., International Geophysics Series, Vol. 77, Academic Press, 317–336.

Cavalieri, D. J., P. Gloerson, C. L. Parkinson, J. C. Comiso, and H. J. Zwally, 1997: Observed hemispheric asymmetry in global sea ice changes. *Science,* **278,** 1104–1106.

Collins, W. D., 2001: Parameterization of generalized cloud overlap for radiative calculations in general circulation models. *J. Atmos. Sci.,* **58,** 3224–3242.

——, P. J. Rasch, B. E. Eaton, B. Khattatov, J.-F. Lamarque, and C. S. Zender, 2001: Simulating aerosols using a chemical transport model with assimilation of satellite aerosol retrievals: Methodology for INDOEX. *J. Geophys. Res.,* **106,** 7313–7336.

——, J. K. Hackney, and D. P. Edwards, 2002a: A new parameterization for infrared emission and absorption by water vapor in the National Center for Atmospheric Research Community Atmosphere Model. *J. Geophys. Res.,* **107,** 8028, doi:10.1029/2000JD000032.

——, P. J. Rasch, B. E. Eaton, D. W. Fillmore, J. T. Kiehl, T. C. Beck, and C. S. Zender, 2002b: Simulation of aerosol distributions and radiative forcing for INDOEX: Regional climate impacts. *J. Geophys. Res.,* **107,** 4664, doi:10.1029/2001JD001365.

——, and Coauthors, 2004: Description of the NCAR Community Atmosphere Model (CAM3). Tech. Rep. NCAR/TN-464+STR, National Center for Atmospheric Research, Boulder, CO, 226 pp.

——, and Coauthors, 2006a: The formulation and atmospheric simulation of the Community Atmosphere Model version 3 (CAM3). *J. Climate,* **19,** 2144–2161.

——, J. M. Lee-Taylor, D. P. Edwards, and G. L. Francis, 2006b: Effects of increased near-infrared absorption by water vapor on the climate system. *J. Geophys. Res.,* in press.

Connolley, W. M., J. M. Gregory, E. C. Hunke, and A. J. McLaren, 2004: On the consistent scaling of terms in the sea-ice dynamics equation. *J. Phys. Oceanogr.,* **34,** 1776–1780.

Craig, A. P., R. L. Jacob, B. Kauffman, T. Bettge, J. Larson, E. Ong, C. Ding, and Y. He, 2005: Cpl6: The new extensible, high-performance parallel coupler for the Community Climate System Model. *Int. J. High Perform. C,* **19,** 309–327.

Danabasoglu, G., W. G. Large, J. J. Tribbia, P. R. Gent, B. P. Briegleb, and J. C. McWilliams, 2006: Diurnal coupling in the tropical oceans of CCSM3. *J. Climate,* **19,** 2347–2365.

Deser, C., A. Capotondi, R. Saravanan, and A. Phillips, 2006: Tropical Pacific and Atlantic variability in CCSM3. *J. Climate,* **19,** 2451–2481.

DeWeaver, E., and C. M. Bitz, 2006: Atmospheric circulation and its effect on Arctic sea ice in CCSM3 at medium and high resolution. *J. Climate,* **19,** 2415–2436.

Dickinson, R. E., K. W. Oleson, G. Bonan, F. Hoffman, P. Thornton, M. Vertenstein, Z.-L. Yang, and X. Zeng, 2006: The Community Land Model and its climate statistics as a component of the Community Climate System Model. *J. Climate,* **19,** 2302–2324.

Drake, J. B., P. W. Jones, and G. R. Carr, 2005: Overview of the software design of the CCSM. *Int. J. High Perform. C,* **19,** 177–186.

Gent, P. R., F. O. Bryan, G. Danabasoglu, K. Lindsay, D. Tsumune, M. W. Hecht, and S. C. Doney, 2006: Ocean chlorofluorocarbon and heat uptake during the twentieth century in the CCSM3. *J. Climate,* **19,** 2366–2381.

Hack, J. J., J. M. Caron, G. Danabasoglu, K. W. Oleson, C. Bitz, and J. Truesdale, 2006: CCSM–CAM3 climate simulation sensitivity to changes in horizontal resolution. *J. Climate,* **19,** 2267–2289.

Harrison, E. F., P. Minnis, B. R. Barkstrom, V. Ramanathan, R. D. Cess, and G. G. Gibson, 1990: Seasonal variation of cloud radiative forcing derived from the Earth Radiation Budget Experiment. *J. Geophys. Res.,* **95,** 18 687–18 703.

Holland, M. M., C. M. Bitz, E. C. Hunke, W. H. Lipscomb, and J. L. Schramm, 2006: Influence of the sea ice thickness distribution on polar climate in CCSM3. *J. Climate,* **19,** 2398–2414.

Houghton, J. T., Y. Ding, D. J. Griggs, M. Noguer, P. J. van der Linden, X. Dai, K. Maskell, and C. A. Johnson, Eds., 2001: *Climate Change 2001: The Scientific Basis.* Cambridge University Press, 944 pp.

Hurrell, J. W., J. J. Hack, A. Phillips, J. Caron, and J. Yin, 2006: The dynamical simulation of the Community Atmospheric Model version 3 (CAM3). *J. Climate,* **19,** 2162–2183.

Kållberg, P., A. Simmons, S. Uppala, and M. Fuentes, 2004: The ERA-40 archive. Tech. Rep. ERA-40 Project Rep. 17, European Centre for Medium-Range Weather Forecasts, Reading, United Kingdom, 35 pp.

Kiehl, J. T., and K. E. Trenberth, 1997: Earth's annual global mean energy budget. *Bull. Amer. Meteor. Soc.,* **78,** 197–208.

——, and P. R. Gent, 2004: The Community Climate System Model, version 2. *J. Climate,* **17,** 3666–3682.

——, C. A. Shields, J. J. Hack, and W. D. Collins, 2006: The climate sensitivity of the Community Climate System Model version 3 (CCSM3). *J. Climate,* **19,** 2584–2596.

Kistler, R., and Coauthors, 2001: The NCEP–NCAR 50-year reanalysis: Monthly means CD-ROM and documentation. *Bull. Amer. Meteor. Soc.,* **82,** 247–267.

Large, W. G., and G. Danabasoglu, 2006: Attribution and impacts of upper-ocean biases in CCSM3. *J. Climate,* **19,** 2325–2346.

Levis, S., G. B. Bonan, M. Vertenstein, and K. W. Oleson, 2004: The Community Land Model's Dynamic Global Vegetation Model (CLM-DGVM): Technical description and user's guide. Tech. Rep. NCAR/TN-459+IA, National Center for Atmospheric Research, Boulder, CO, 50 pp.

Levitus, S., and Coauthors, 1998: *Introduction*. Vol. 1, *World Ocean Database 1998*, NOAA Atlas NESDIS 18, 346 pp.

Libscomb, W. H., and E. C. Hunke, 2004: Modeling sea-ice transport using incremental remapping. *Mon. Wea. Rev.,* **132,** 1341–1354.

Lin, S.-J., 2004: A vertically Lagrangian finite-volume dynamical core for global models. *Mon. Wea. Rev.,* **132,** 2293–2307.

——, and R. B. Rood, 1996: Multidimensional flux-form semi-Lagrangian transport schemes. *Mon. Wea. Rev.,* **124,** 2046–2070.

Meehl, G. A., J. M. Arblaster, D. M. Lawrence, A. Seth, E. K. Schneider, B. P. Kirtman, and D. Min, 2006: Monsoon regimes in the CCSM3. *J. Climate,* **19,** 2482–2495.

Ohlmann, J. C., 2003: Ocean radiant heating in climate models. *J. Climate,* **16,** 1337–1351.

Oleson, K. W., G. B. Bonan, C. Schaaf, F. Gao, Y. Jin, and A. Strahler, 2003: Assessment of global climate model land surface albedo using MODIS data. *Geophys. Res. Lett.,* **30,** 1443, doi:10.1029/2002GL016749.

——, and Coauthors, 2004: Technical description of the Community Land Model (CLM). Tech. Rep. NCAR/TN-461+STR, National Center for Atmospheric Research, Boulder, CO, 174 pp.

Otto-Bliesner, B. L., E. C. Brady, G. Clauzet, R. A. Tomas, S. Levis, and Z. Kothavala, 2006: Last Glacial Maximum and Holocene climate in CCSM3. *J. Climate,* **19,** 2526–2544.

Perovich, D. K., T. C. Grenfell, B. Light, and P. V. Hobbs, 2002: Seasonal evolution of the albedo of multiyear Arctic sea ice. *J. Geophys. Res.,* **107,** 8044, doi:10.1029/2000JC000438.

Persson, P. O. G., C. W. Fairall, E. L Andreas, P. S. Guest, and D. K. Perovich, 2002: Measurements near the Atmospheric Surface Flux Group tower at SHEBA: Near-surface conditions and surface energy budget. *J. Geophys. Res.,* **107,** 8045, doi:10.1029/2000JC000705.

Rasch, P. J., M. C. Barth, J. T. Kiehl, S. E. Schwartz, and C. M. Benkovitz, 2000: A description of the global sulfur cycle and its controlling processes in the National Center for Atmospheric Research Community Climate Model, Version 3. *J. Geophys. Res.,* **105,** 1367–1385.

——, W. D. Collins, and B. E. Eaton, 2001: Understanding the Indian Ocean Experiment (INDOEX) aerosol distributions with an aerosol assimilation. *J. Geophys. Res.,* **106,** 7337–7356.

Rayner, N. A., D. E. Parker, E. B. Horton, C. K. Folland, L. V. Alexander, D. P. Powell, E. C. Kent, and A. Kaplan, 2003: Global analyses of sea surface temperature, sea ice, and night marine air temperature since the late nineteenth century. *J. Geophys. Res.,* **108,** 4407, doi:10.1029/2002JD002670.

Rothrock, D. A., Y. Yu, and G. A. Maykut, 1999: Thinning of the arctic sea-ice cover. *Geophys. Res. Lett.,* **26,** 3469–3472.

Schmidt, G. A., C. M. Bitz, U. Mikolajewicz, and L. B. Tremblay, 2004: Ice-ocean boundary conditions for coupled models. *Ocean Modell.,* **7,** 59–74.

Smith, R. D., and P. R. Gent, 2002: Reference manual for the Parallel Ocean Program (POP), ocean component of the Community Climate System Model (CCSM2.0 and 3.0). Tech. Rep. LA-UR-02-2484, Los Alamos National Laboratory. [Available online at http://www.ccsm.ucar.edu/models/ccsm3.0/pop.]

——, S. Kortas, and B. Meltz, 1995: Curvilinear coordinates for global ocean models. Tech. Rep. LA-UR-95-1146, Los Alamos National Laboratory, 50 pp.

Timmermann, R., A. Worby, H. Goosse, and T. Fichefet, 2004: Utilizing the aspect sea ice thickness data set to evaluate a global coupled sea ice-ocean model. *J. Geophys. Res.,* **109,** C07017, doi:10.1029/2003JC002242.

Williamson, D. L., 2002: Time-split versus process-split coupling of parameterizations and dynamical core. *Mon. Wea. Rev.,* **130,** 2024–2041.

Willmott, C. J., and K. Matsuura, 2000: Terrestrial air temperature and precipitation: Monthly and annual climatologies. [Available online at http://climate.geog.udel.edu/~climate.]

Yeager, S. G., C. A. Shields, W. G. Large, and J. J. Hack, 2006: The low-resolution CCSM3. *J. Climate,* **19,** 2545–2566.

Zhang, Y. C., W. B. Rossow, A. A. Lacis, V. Oinas, and M. I. Mishchenko, 2004: Calculation of radiative fluxes from the surface to the top of atmosphere based on ISCCP and other global data sets: Refinements of the radiative transfer model and the input data. *J. Geophys. Res.,* **109,** D19105, doi:10.1029/2003JD004457.